To the Graduate Council:

I am submitting herewith a thesis written by D. Leslie Burwell entitled "Rotor Speed Control for a Demonstrator Helicopter Engine". I have examined the final copy of this thesis for form and content and recommend that it be accepted in partial fulfillment for the requirements for the degree of Master of Science with a major in Electrical Engineering.

Bruce W. Bomar, Major Professor

We have read this thesis
and recommend its acceptance:

Roy D. Joseph

L. Montgomery Smith

Accepted for the Council:

Vice Provost
and Dean of The Graduate School

STATEMENT OF PERMISSION TO USE

In presenting this thesis in partial fulfillment of the requirements for a Master's degree at The University of Tennessee, Knoxville, I agree that the Library shall make it available to borrowers under rules of the Library. Brief quotations from this thesis are allowable without special permission, provided that accurate acknowledgment of source is made.

Permission for extensive quotation from or reproduction of this thesis may be granted by my major professor, or in his absence, by the Head of Interlibrary Services when, in the opinion of either, the proposed use of the material is for scholarly purposes. Any copying or use of the material in this thesis for financial gain shall not be allowed without my written permission.

Signature D. Leslie Burnell

Date May 19, 1990

ROTOR SPEED CONTROL FOR A DEMONSTRATOR HELICOPTER ENGINE

A Thesis

Presented for the

Master of Science

Degree

The University of Tennessee, Knoxville

D. Leslie Burwell

August 1990

ACKNOWLEDGMENTS

I would like to express my appreciation to Dr. Bruce W. Bomar and Dr. Roy D. Joseph for their advice and assistance in completing the Electrical Engineering program at The University of Tennessee Space Institute (UTSI). I also appreciate Dr. L. Montgomery Smith's review of the material.

In particular, I would like to thank Glen High for suggesting a topic and reviewing thesis content. Also a special thanks to Branch Crooks for his encouragement and review of the material when I was getting started.

Finally, I would like to thank my husband, Al Burwell and son, Michael Burwell for their patience and support.

ABSTRACT

Since military helicopters of today must operate in hostile environments and carry out intricate maneuvers, it is required that their engine and rotor systems be under automatic control. During early concept testing of a demonstrator engine for such applications, a simple controller is needed to maintain a fixed power turbine speed and insure the general stability of the engine and rotor.

A mathematical model for the helicopter plant is a necessary first step in the design of a controller suitable for demonstration testing. In this thesis a linearized model of the plant was developed by expanding the governing equations about a quiescent operating point. This linear model was then analyzed in both the frequency domain (Bode) and the time domain to determine the plant's characteristics. Special attention was focused on the two major destabilizing effects for an engine and rotor system, which occur at the rotor and power turbine natural frequency and upon autorotation.

Controller design goals were selected to include a phase margin in excess of 45°, gain margin of 6 dB, and steady-state accuracy within 15%. The uncompensated plant was analyzed first and different types of simple compensation were selected to fulfill the design goals. A second order notch filter was added to the controller to satisfy the

torsional stability requirements without compromising the rotor speed governor's transient response. Good system performance was achieved with a bandwidth, evaluated at the gain crossover frequency, of 3 rad/sec (0.48 Hz).

The simple controller designed here provides a suitable governor for the demonstrator engine and forms a baseline for continuing studies involving sophisticated control techniques applied to more advanced helicopter systems.

TABLE OF CONTENTS

CHAPTER		PAGE
I.	INTRODUCTION	1
II.	THE PLANT DYNAMICS	9
	SYSTEM DESCRIPTION	9
	GAS GENERATOR MODEL	11
	POWER TURBINE MODEL	18
	ENGINE MODEL	22
	ROTOR MODEL	24
	HYDROMECHANICAL MODEL	29
	PLANT MODEL	30
III.	MODEL PARAMETERS	33
	INTRODUCTION	33
	ENGINE AND ROTOR CONSTANTS	33
	ENGINE PERFORMANCE MODEL	34
	GAS GENERATOR GOVERNOR DESIGN	39
	PLANT TRANSFER FUNCTION	40
IV.	THE ANALYSIS	42
	INTRODUCTION	42
	TORSIONAL RESONANCE	42
	AUTOROTATION	43
	DESIGN GOALS	44
	MATLAB	47
V.	CONTROLLER DESIGN	48
	INTRODUCTION	48
	PLANT ANALYSIS	48
	COMPENSATOR DESIGN	53
	RESULTS AT EACH POWER LEVEL	66
	RESULTS FOR THE DECOUPLED ROTOR	69
	FINAL RESULTS	72
VI.	DISCUSSION	73
LIST OF REFERENCES		74
VITA		79

LIST OF TABLES

TABLE		PAGE
1.	Inertias, spring constant and 100% speeds of the plant.	34
2.	Parameter variation with changes in power setting, at standard day conditions.	36
3.	Design goals for the engine and rotor system.	47
4.	Steady-state error of the uncompensated plant.	51
5.	Summary of the behavior of the uncompensated plant.	53
6.	Results of variation in compensator values for the plant at 750 SHP	65
7.	Gains and time constants selected for the coupled rotor system	66
8.	The final results for the coupled rotor system with selected compensator values	68
9.	Summary for the decoupled rotor system with the gains and time constants shown in Table 10	71
10.	Gains and time constants for data in Table 9.	71
11.	The final results for the system with selected compensator values shown in Table 12	72
12.	Gains and time constants for data in Table 11.	72

LIST OF FIGURES

FIGURE		PAGE
1.	Typical engine control system	3
2.	Speed governor control loop	4
3.	The components of a gas turbine engine	10
4.	Simplified gas generator model showing pressure and temperature effects	15
5.	Derivation of the transfer function for gas generator speed to fuel flow using block diagram manipulation	16
6.	Block diagram showing compressor pressure effects on the gas generator model	18
7.	Torque characteristics of the gas generator	19
8	Torque characteristics of the free power turbine	20
9.	The power turbine model without loading effects	22
10.	The engine model without loading effects	23
11.	The rotor dynamics	25
12.	Three mass rotor representation	26
13.	Two mass rotor representation	27
14.	The rotor model	29
15.	The HMU dynamics	30
16.	Block diagram of the plant	32
17.	Frequency response of $\frac{\Delta N_p}{\Delta Q_{pg}}$ at 750 SHP	43
18.	Open-loop frequency response of the plant with the rotor coupled, at each power level	49
19.	Open-loop frequency response of the plant with the rotor decoupled	51
20.	Closed-loop step response of the plant at 750 SHP	52

21. Block diagram of the system..... 54

22. Frequency response of $\frac{1}{T_p s + 1}$ with phase lag of 0.8 sec 57

23. Open-loop frequency response of the system at 750 SHP with a phase lag of 0.8 sec 58

24. Closed-loop step response of the system at 750 SHP with a phase lag of 0.8 sec 59

25. Open-loop frequency response of the system at 750 SHP with a phase lag of 0.25 sec 60

26. Open-loop frequency response of the system at 750 SHP with T_p=0.25 and K_p=2.85 61

27. Frequency response of $\frac{s^2 + 2\zeta_{lag}\,\omega_n\, s + \omega_n^2}{s^2 + 2\zeta_{lead}\,\omega_n\, s + \omega_n^2}$ with ω_n=17.3, ζ_{lead}=1.5 and ζ_{lag}=0.15 63

28. Open-loop frequency response of the system at 750 SHP with K_p=2.85, T_p=0.25, ω_n=17.3, ζ_{lead}=1.5 and ζ_{lag}=0.15 64

29. Block diagram showing compensator..... 66

30. Open-loop frequency response of the system at each power level with selected compensation 67

31. Closed-loop step response of the system at each power level with selected compensation 68

32. Open-loop frequency response of the decoupled rotor system with the compensation selected for the coupled rotor system 70

33. Open-loop frequency response of the system with selected compensation 70

34. Closed-loop step response of the decoupled rotor system with selected compensation 71

LIST OF SYMBOLS

PHYSICAL CONSTANTS AND ABBREVIATIONS

°C	Degree Celsius
Δ	Delta
°	Degrees
f	Function
∂	Partials
%	Per cent
BW	Bandwidth (rad/sec)
config	The configuration of the engine and rotor system will either be CR for coupled rotor or DR for decoupled rotor.
CR	Coupled rotor
dB	Decibels
DR	Decoupled rotor
ft-lb	Foot-pounds
GM	Gain margin (dB)
GR	Gain at the resonant peak (dB)
HMU	Hydromechanical unit
hr	Hours
Hz	Hertz
in. Hg.	Inch of mercury
msec	Seconds X 10^{-3}
N/A	Not applicable
N/D	Not defined or undefined
PM	Phase margin (°)

pph	Pounds per hour (lb/hr)
psi	Pounds per square inch
rad/sec	Radians per second
rpm	Revolution per minute
sec	Seconds
SHP	Shaft horsepower
ss-err	Steady-state error (%)
WFR	Ratio of fuel flow to pressure, $\Delta(W_f/P)$

CONTROLLER CONSTANTS AND SYMBOLS

K_g	Gas generator gain (WFR/%N_g)
$K_{g\text{-conv}}$	Controller gain equal to 2.207×10^{-3}, which is 100%N_g/45,306rpm
K_p	Proportional gain (%N_g/%N_p)
$K_{p\text{-conv}}$	Controller gain equal to 2.756, which is 45,306rpm/100%N_g X 100%N_p/16,438rpm
T_p	Phase lag time constant (sec)
ω_n	Undamped resonant frequency (rad/sec)
ζ_{lead}	Damping ratio for the lead function
ζ_{lag}	Damping ratio for the lag function

PLANT CONSTANTS AND SYMBOLS

B_p	Damping of the power turbine, equivalent to $-\frac{\partial Q_p}{\partial N_p}$ (ft-lb/rpm)

B_r	Damping of the rotor system, equivalent to $-\frac{\partial Q_r}{\partial N_r}$ (ft-lb/rpm)
J_g	Gas generator moment of inertia (ft-lb-sec/rpm)
J_p	Power turbine moment of inertia (ft-lb-sec/rpm)
J_r	Rotor moment of inertia (ft-lb-sec/rpm)
K_t	Spring constant (ft-lb/rpm)
K_e	Gas generator gain (rpm/pph)
N_g	Gas generator speed (rpm)
N_{gerr}	Gas generator speed error between the reference and feedback speed (rpm)
N_{go}	Gas generator speed about some operating point (rpm)
N_{gset}	Gas generator speed reference commanded from the electronic control (rpm)
N_p	Power turbine speed (rpm)
N_{perr}	Power turbine speed error (rpm)
N_{po}	Power turbine speed about some operating point (rpm)
N_{pset}	Power turbine speed reference commanded by the pilot (rpm)
P	Compressor outlet pressure (psi)
P_o	Compressor inlet pressure about some operating point (psi)
Q_d	Torque induced by a disturbance to the rotor (ft-lb)
Q_g	Gas generator torque (ft-lb)
Q_p	Power turbine torque (ft-lb)
Q_{pg}	Power turbine torque due to the gas generator section of the engine (ft-lb)
Q_r	Rotor torque (ft-lb)

Q_s	Torque due to the transmission shaft stiffness (ft-lb)
T	Gas generator turbine inlet temperature (°C)
T_e	Engine time constant (sec)
T_h	Time constant for the hydromechanical unit (sec)
T_o	Gas generator turbine inlet temperature about some operating point (°C)
W_f	Fuel flow (lb/hr)
W_{fo}	Fuel flow about some operating point (lb/hr)
ω_r	Resonant frequency of the coupled rotor and power turbine (rad/sec)
$\varnothing_p$	angular position of the power turbine (radians)
$\varnothing_r$	angular position of the rotor (radians)

CHAPTER I

INTRODUCTION

The purpose of this study is to design the controller for a helicopter engine demonstrator program. The goal of this program is to demonstrate the flight capability of a prototype turboshaft engine. To demonstrate engine performance, operability, durability and new component technologies, prototype engine development is needed [1]*. How well these capabilities are demonstrated influence whether there is any funding for full-scale engine development.

Airframe development takes less time than engine development and often the engine development precedes the airframe selection by several years. The helicopter manufacturer for this program has not been selected and the flight test is supported by modifying an existing helicopter with the prototype engine. To demonstrate flight capability of the engine, a simple controller is required whose complexity matches the complexity of the demonstrator helicopter. In the past, a simple controller has been obtained by modifying an existing analog control, enabling the conversion to existing hardware with minimum cost and development effort.

*Numbers in brackets refer to similarly numbered references in the List of References.

In a helicopter application the pilot selects a desired power turbine speed and then commands the collective pitch angle, or average angle of attack, of the (main) rotor blades to control the lift. In a turboshaft engine, the turbine power available to produce the torque for the rotor is measured in terms of shaft horsepower (SHP). The maximum power output of the demonstrator engine is 750 shaft horsepower.

Electronic engine control must regulate the speed of the engine, as set by the pilot, without exceeding the safe operating limits of the engine. This is accomplished by continuously measuring the actual engine speeds, temperatures and pressures and adjusting the fuel flow command to the hydromechanical unit (HMU), which provides fuel to the engine. An overall description of such an engine control system is shown in Figure 1.

There are several control loops implemented in an electronic engine control. The prime function of this controller, also referred to as speed governor, is to maintain a constant power turbine speed which results in a constant rotor speed, with the pilot modulating the SHP by changing the collective pitch angle of the rotor blades. The speed governor acts to maintain a constant rotor speed regardless of induced engine loads. Induced engine loading can be caused by external disturbances such as wind gusts, or pilot-initiated disturbances such as collective pulls where

the collective pitch of the rotor blades is rapidly increased, or maneuvers.

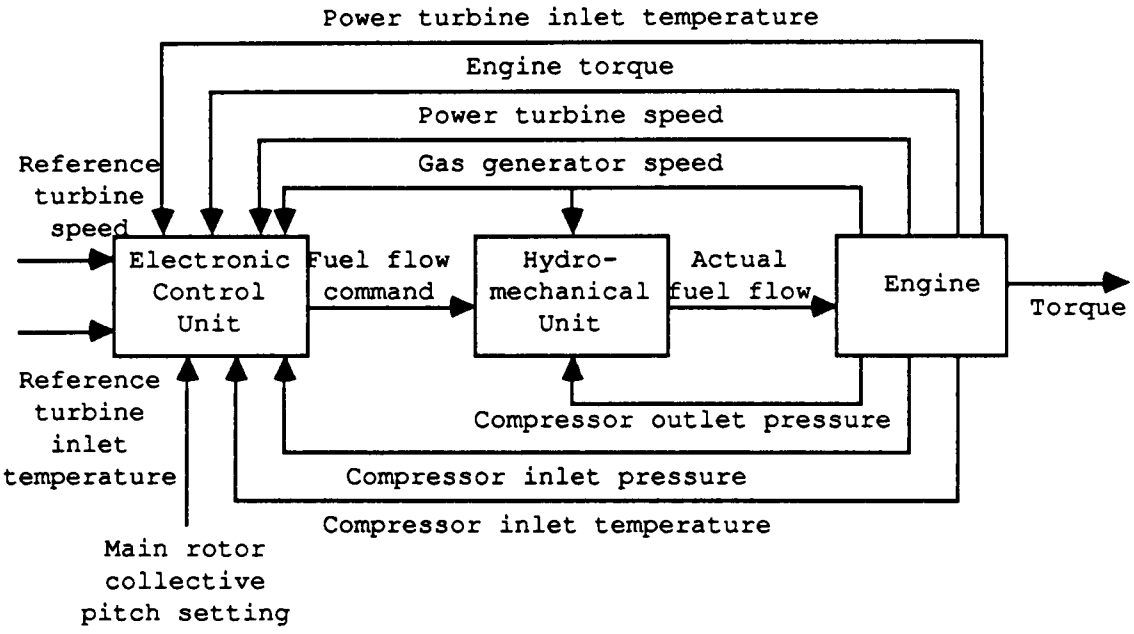

Figure 1. Typical engine control system.

A simplified block diagram of the electronic control's speed governor is shown in Figure 2. A measurement of the actual speed is compared to the engine speed commanded by the pilot, in order to generate an error signal that is used to produce a fuel flow command to the HMU. The rotor speed governor must be designed to minimize the steady-state speed error and produce a good transient response. A large steady-state error or sluggish response can cause the system to be difficult or impossible to control during maneuvers. The

speed governor design also must consider the two effects on the engine and rotor system which can lead to instability.

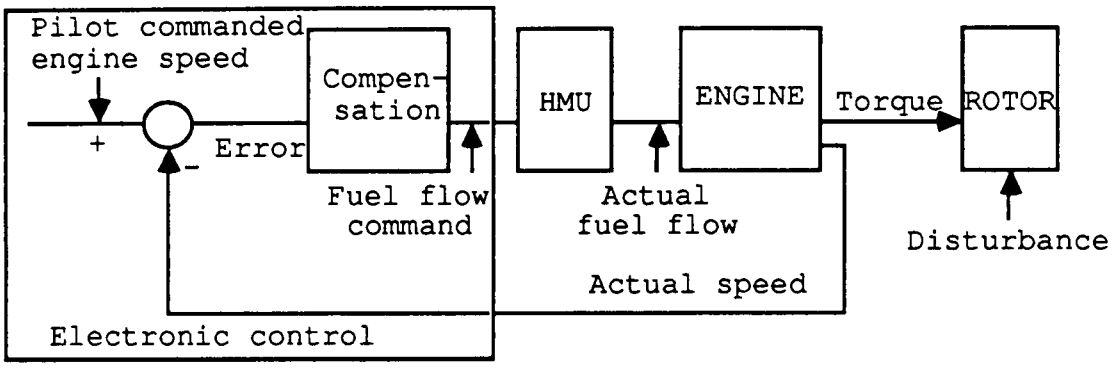

Figure 2. Speed governor control loop.

The first instability occurs at the torsional resonant frequency, or natural frequency of the rotor coupled to the power turbine. When this occurs the rotor is being driven by the engine and the SHP is greater than zero. The rotor acts as a spring and will oscillate since there is a large mismatch between the engine's power turbine inertia and the rotor inertia. The natural frequency of the rotor and engine is within the passband of the HMU, resulting in torsional resonant amplification at this critical frequency. A major task of the speed governor is to attenuate these oscillations and prevent the propagation of this destructive mode. The torsional dynamic interaction between the rotor and power

turbine requires special consideration in the controller design.

The other destabilizing effect occurs when the rotor decouples from the engine. A large increase in system loop gain is caused by the reduction in rotor inertia. The rotor decouples from the engine when the engine is no longer providing power to turn the rotor blades and the power supplied by the engine's power turbine is less than the power being supplied to the rotor blades by the surrounding air. Hence this condition is referred to as autorotation since the rotor is driven by the surrounding air. The rotor decouples during descent, a dive maneuver, and if a failure causes the engine to become inoperative.

Most work related to the development of a rotor speed governor appears in the Journals of the American Helicopter Society, or in government funded research project reports. The torsional instability problem which this paper addresses was recognized as early as 1964 and considered at that time to be minor and acceptable to pilots [2]. Starting in the 1970's helicopters were required to perform more severe maneuvers and HMU's were being designed with a higher gain to provide higher performance, resulting in an amplification of the torsional oscillations to an unacceptable level. Studies [2,3,4] by the major helicopter manufacturers have been carried out to solve this problem.

The parameters found to have a significant effect on torsional stability were the main rotor lag damping, the torsional stiffness of the main rotor shaft, and controller gain. Incorporating solutions directly in the controller in the form of proportional and first order phase lag damps the torsional resonant oscillations but compromises the steady-state and transient response of the system [2].

With the development of electronic engine controls in the mid-1970's, research has increased in utilizing electronic control to dampen these oscillations so the HMU does not react to them. In 1975, a prototype analog electronic engine control, being used to support a test rig, was modified with compensation in the form of a notch filter and found to provide satisfactory torsional stability without compromising system performance [4]. In the early 1980's a research digital engine control was designed to permit implementation and evaluation of complex logic to investigate utilizing the emerging digital controls technology for helicopter engines to improve maneuverability and reduce pilot workload [5]. Today, electronic controls are being designed to reduce pilot workload by performing ever increasing numbers of functions.

This thesis determines the stabilizing compensation that also provides good steady-state and transient performance. The physical characteristics of the uncompensated plant, consisting of the engine, rotor and HMU are studied to obtain

CHAPTER II

THE PLANT DYNAMICS

SYSTEM DESCRIPTION

This chapter describes the physical behavior of the engine and rotor system. Since a helicopter's performance involves the interaction of the engine and rotor, the design of a rotor speed governor requires that each of these components be modeled.

A gas turbine engine in its simplest form consists of a gas generator composed of a compressor, combustor, and turbine on a single shaft as shown in Figure 3a. Air enters the engine and rises in temperature as the pressure increases in the compressor. Fuel is added to the high pressure air in the combustor to produce a mixture, or gas at a higher temperature and with increased heat content. Expansion of this hot gas in the turbine delivers the power that is used to produce work to turn the shaft that drives the compressor.

In this configuration the gas generator does not provide useful work for an aircraft since most of the fuel energy is converted into high speed rotational energy to turn the compressor. A second turbine is added on the same shaft to produce additional energy that is converted to useful work in a single, fixed shaft arrangement. A free (mechanically

transient response of the engine/rotor speed loop which is measured at the low frequency zero decibel crossover. Thus the notch filter provides stability without compromising system performance. The effect each type of compensation has on the plant is discussed.

Once the compensation is selected for the high power setting, Bode and step response plots are made at each power setting to show performance across the entire operating range. The compensation chosen for the coupled rotor case is shown to create instability in the decoupled rotor case. Therefore a different compensation in the form of proportional and phase lag only is developed for the decoupled rotor case.

This paper provides a baseline for further control development for military helicopters. Sources describing helicopter engine controller design are limited. This paper serves as an introduction to the helicopter controller development. Only basic concepts, as they apply to helicopter engine controls, are discussed. Modern helicopters require engine controls that consider advanced control concepts to improve aircraft handling qualities and reduce pilot workload. Once the helicopter dynamics are defined, these advanced control concepts can be considered fully.

a mathematical model for analysis. These equations are then combined and a linear perturbation analysis performed about specified power settings. Classical methods, in the form of frequency and step response analysis using MATLAB [6] are used to minimize design time.

To permit analysis of the system, its model is linearized at four engine power settings, representative of the full operating range of the engine: high, intermediate, low and zero shaft horsepower. The coupled rotor is studied at each of these power points. Plots are made of the zero SHP case with the rotor coupled and decoupled. The condition of zero SHP is included with the plots of the coupled rotor to verify stability across the entire operating range. Only the zero SHP or no load condition is of any interest for the decoupled rotor case since if any load is applied to the power turbine the SHP is greater than zero and the rotor is considered coupled.

Bode and step response plots of the uncompensated plant are studied and dynamic compensation selected that meets the design goals. Compensation in the form of phase lag, in cascade with the plant is shown to attenuate the torsional resonant oscillations, but with poor steady-state accuracy and transient response. A second order notch filter is designed in the feedback loop to provide stability, by attenuating the resonant peak. Proportional is then added in cascade to increase the bandwidth, an indication of the

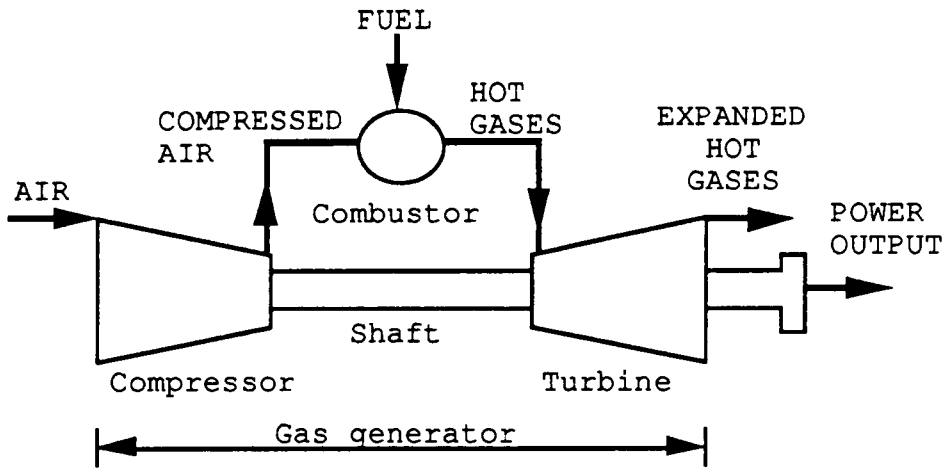

(a) gas generator section of a gas turbine engine

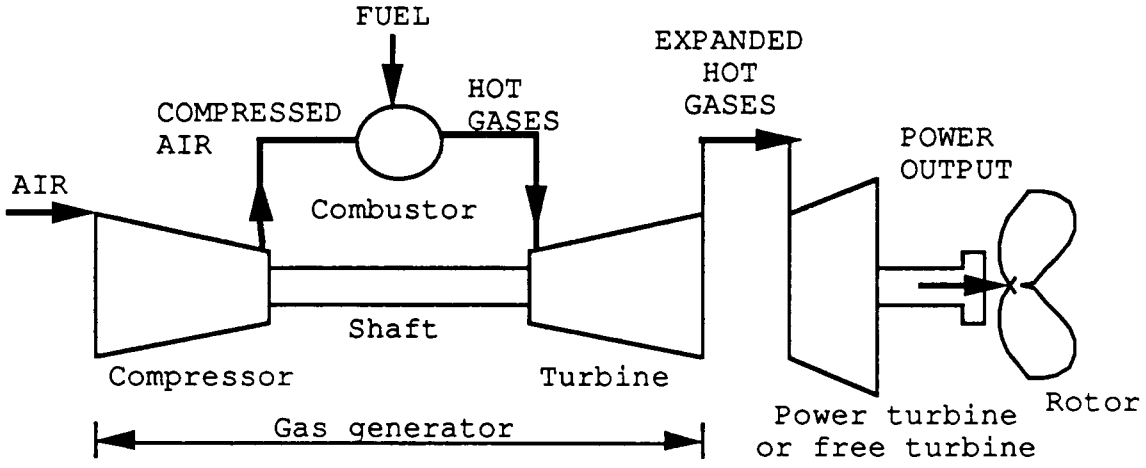

(b) turboshaft engine with a free power turbine

Figure 3. The components of a gas turbine engine.

independent) power turbine is added in a twin-shaft arrangement, as shown in Figure 3b [7]; it is not physically connected to the gas generator and turns at a different speed than the gas generator. The demonstrator engine is a free

power turbine engine. In a helicopter application, the shaft of the free power turbine drives the helicopter rotor.

Of major interest for the gas turbine engine is the dependence of gas generator speed on fuel flow and the power turbine speed on torque. For a turboshaft engine the primary input is fuel flow and the primary output is rotor speed. System equations for the gas generator, free power turbine and rotor are developed in the following sections. The system equations for the gas generator and power turbine are combined using block diagram manipulation to produce a linear perturbation model of the engine. Since the HMU provides fuel to the engine and will amplify any instability caused by the interaction of the engine and rotor system, the HMU dynamics are also described and modeled. Then the engine, rotor and HMU are combined into a linear model that is used to design the rotor speed governor.

GAS GENERATOR MODEL

In this section the physical laws which relate the variables of the gas generator: turbine inlet temperature (T), compressor outlet pressure (P), fuel flow (W_f), gas generator speed (N_g), gas generator inertia (J_g) and gas generator torque (Q_g) are described. From these physical laws, the non-linear equations are developed that describe the operation of the gas generator section of a gas turbine engine. A Taylor series expansion about a quiescent operating

point is performed to obtain a linear model, which is then represented in block diagram form.

The pressure and temperature of the hot gases from the gas generator depend on the gas generator speed and fuel flow. Within a linear operating range, the temperature of the hot gases will increase due to the addition of fuel, resulting in a pressure increase due to the rise in temperature. This increase in fuel flow will also cause the gas generator speed to increase, until the turbine chokes. When the turbine chokes, the air flow will remain constant and the temperature will increase. As a result of the temperature rise, the pressure will increase rapidly. Hence, the non-linear behavior of the gas generator's pressure and temperature can be represented functionally as

$$P = P(W_f, N_g)$$

$$T = T(W_f, N_g) \ .$$

These relations can be linearized by performing a Taylor series expansion about an operating point (W_{fo}, N_{go}) [8].

$$\Delta P = (\Delta W_f)\frac{\partial P(W_{fo}, N_{go})}{\partial W_f} + (\Delta N_g)\frac{\partial P(W_{fo}, N_{go})}{\partial N_g} \qquad (1)$$

$$\Delta T = (\Delta W_f)\frac{\partial T(W_{fo}, N_{go})}{\partial W_f} + (\Delta N_g)\frac{\partial T(W_{fo}, N_{go})}{\partial N_g} \ , \qquad (2)$$

where the perturbations about the steady-state conditions are given by,

$$\Delta P = P - P_o$$

$$\Delta T = T - T_o$$

$$\Delta W_f = W_f - W_{fo}$$

$$\Delta N_g = N_g - N_{go} \ .$$

Equations 1 and 2 are only valid for small deviations from the steady-state operating point. All partials will be evaluated at standard day, sea level static conditions. Standard day conditions are defined as a day on which the ambient temperature is 59° Fahrenheit, or 15° Celsius and the barometric pressure is 29.92 in.Hg. For comparison of engine performance data to known standard performance or to other engines, all observed gas turbine engine performance data is converted to static conditions on a standard day at sea level.

The torque, Q_g required to turn the gas generator is given by

$$Q_g = J_g \dot{N}_g \ , \qquad (3)$$

where J_g is the polar moment of inertia of the gas generator. This equation governs the rotational motion of a rigid body about a fixed axis and is the rotational equivalent of Newton's Law.

The torque that is available through the engine is also a function of fuel flow and gas generator speed. This non-linear behavior of the gas generator can be represented functionally [9] as

$$Q_g = Q_g(W_f, N_g) \quad .$$

This leads to the representation of Equation 3 as

$$\dot{N}_g = \frac{1}{J_g} Q_g(W_f, N_g) \quad . \tag{4}$$

By performing a Taylor series expansion about an operating point (W_{fo}, N_{go}) Equation 4 can be linearized

$$\Delta\dot{N}_g = \frac{1}{J_g}\left[\Delta W_f \frac{\partial Q_g(W_{fo}, N_{go})}{\partial W_f} + \Delta N_g \frac{\partial Q_g(W_{fo}, N_{go})}{\partial N_g}\right] \quad . \tag{5}$$

In terms of the Laplace Transform, Equation 5 becomes

$$\Delta N_g = \frac{1}{sJ_g}\left[\Delta W_f \frac{\partial Q_g(W_{fo}, N_{go})}{\partial W_f} + \Delta N_g \frac{\partial Q_g(W_{fo}, N_{go})}{\partial N_g}\right] \quad . \tag{6}$$

Equations 1, 2 and 6 can be represented in block diagram form as shown in Figure 4.

The block diagram shown in Figure 4 was reduced to obtain a simple mathematical description that represents the physical system in transfer function notation. The gas generator model will be combined with the power turbine model to produce a simple engine model. Studies [11,20] present similar models without showing their derivation. The development shown here is based on the physical behavior of the engine and thereby aids in understanding how the engine model was developed.

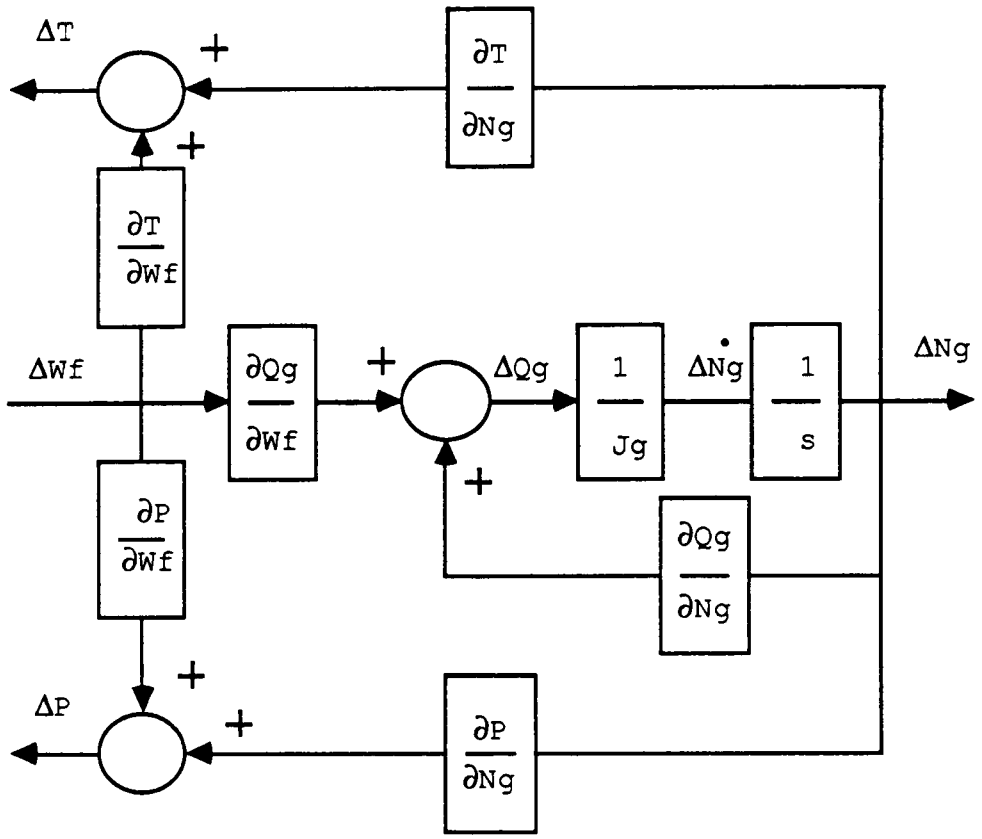

Figure 4. Simplified gas generator model showing pressure and temperature effects.

The closed-loop transfer function for the gas generator, $\Delta N_g/\Delta W_f$ was derived by block diagram manipulation from Figure 4 by first moving the block for $\partial Q_g/\partial W_f$ inside the summing junction [10] as shown in Figure 5a. For constant torque where, $Q_g = K = Q_g(W_f, N_g)$, from differential calculus,

$$\frac{dW_f}{dN_g} = \frac{-\partial Q_g/\partial N_g}{\partial Q_g/\partial W_f} \cdot \qquad (7)$$

Substitution of Equation 7 into Figure 5a yields the block diagram shown in Figure 5b.

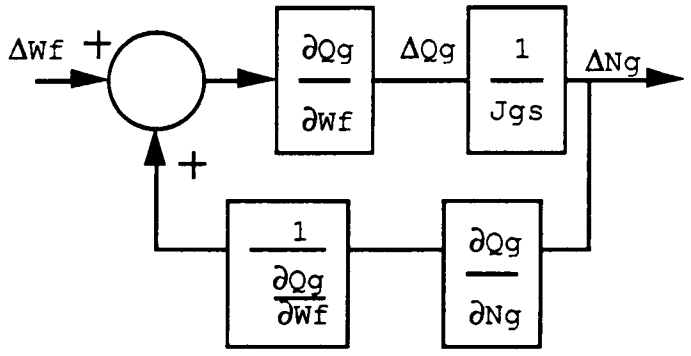

a. After manipulation into standard form

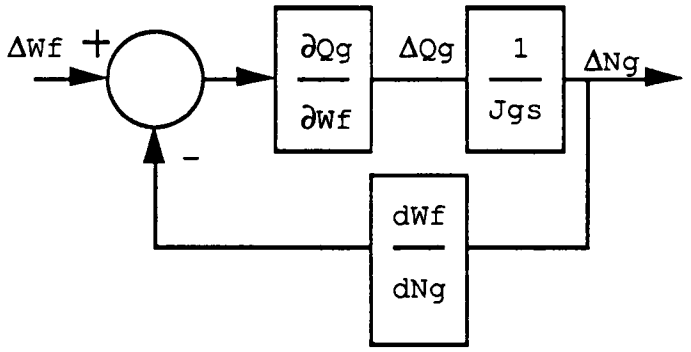

b. After substitution of Equation 7.

Figure 5. Derivation of the transfer function for gas generator speed to fuel flow using block diagram manipulation.

The closed-loop transfer function from Figure 5b is

$$\frac{\Delta N_g(s)}{\Delta W_f(s)} = \frac{dN_g/dW_f}{[J_g s \; / -(\partial Q_g/\partial N_g)] + 1} \quad \text{or} \tag{8}$$

$$\frac{\Delta N_g(s)}{\Delta W_f(s)} = \frac{K_e}{(T_e s + 1)} , \tag{9}$$

where K_e is the gas generator gain and T_e the engine time constant.

The temperature, ΔT shown in Figure 4 can be neglected since it's effect is instantaneous when compared to the other dynamics [11]. Therefore, this path is removed from the block diagram. The pressure effects can not be neglected since the HMU is designed to schedule $\Delta(W_f/P)$ as a function of the gas generator speed error. For this ratio to remain constant, as fuel flow increases, the pressure must increase. In fact, a rise in fuel flow causing gas generator speed to increase, will cause pressure to increase. Since it is a change in the ratio of fuel flow to pressure, which changes the quantity of fuel supplied to the engine, the differential can be found as

$$\Delta W_f = P \; \Delta(W_f/P) + (W_f/P) \; \Delta P \; . \tag{10}$$

Equation 10 is combined with Equation 1 and 9 and represented in block diagram form in Figure 6, after standard block diagram manipulation.

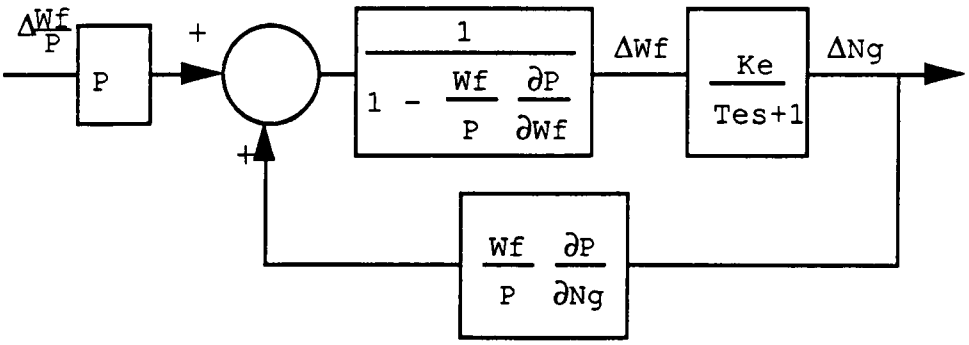

Figure 6. Block diagram showing compressor pressure effects on the gas generator model.

POWER TURBINE MODEL

In this section the physical laws which relate the variables of the power turbine: power turbine speed (N_p), power turbine inertia (J_p), power turbine torque (Q_p), fuel flow (W_f) and gas generator speed (N_g) are described. Non-linear equations are developed that describe the operation of the free power turbine section of a gas turbine engine. A Taylor series expansion about a quiescent operating point is performed to obtain a linear model, which is represented in block diagram form.

In a helicopter application a second turbine is added in a free power turbine arrangement, to produce excess energy that is available from the power turbine to drive a rotor. Since the power turbine is driven by the exhaust discharge from the gas generator path, there exists a fluidic connection between the gas generator and power turbine that simplifies the clutching problem during autorotation.

If the output shaft power is provided by a second turbine in series with the gas generator turbine in a single-shaft arrangement, the compressor of the gas generator runs at a multiple of the load speed which is fixed by the transmission gear ratio. A reduction in load speed will cause a reduction in turbine speed, resulting in a reduction of compressor speed since they are coupled on the same shaft. This results in a reduction in mass flow of air to the turbine, and hence a reduction in the resultant load torque as shown in Figure 7. This arrangement is not desirable for a helicopter rotor since a reduction in load speed causes a reduction in output torque.

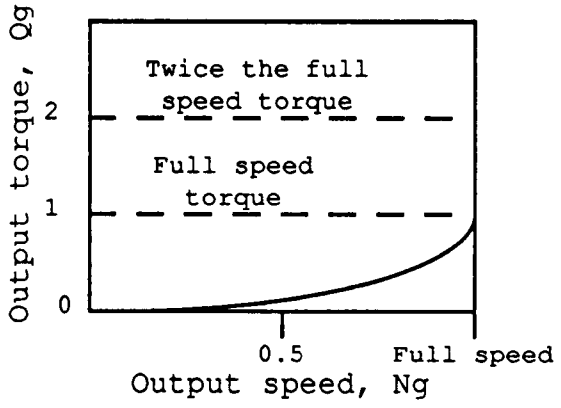

Figure 7. Torque characteristics of the gas generator.

A free power turbine arrangement has a more favorable torque characteristic than a fixed shaft engine since the

engine's power output can be changed to maintain a constant rotor speed regardless of the rotor load. As shown in Figure 8, a reduction in load speed results in an increase in torque, with a stall torque of 2 to 3 times the torque delivered at full speed being possible. The gas generator supplies a constant flow of air to the power turbine regardless of the free power turbine's speed variation due to load changes.

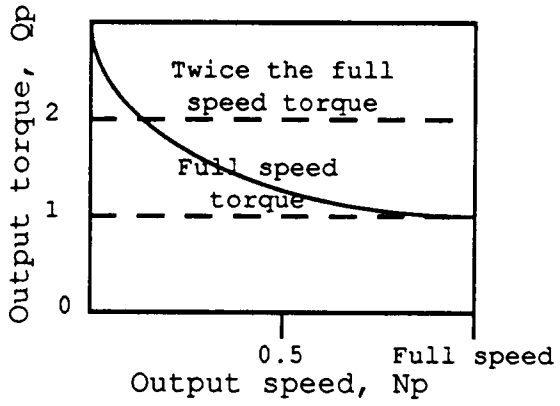

Figure 8. Torque characteristics of the free power turbine.

If there is no load connected to the power turbine the torque, Q_p required to only turn the power turbine is given by

$$Q_p = J_p \dot{N}_p \quad , \tag{11}$$

where J_p is the polar moment of inertia of the power turbine.

The torque delivered by the power turbine is also a function of the gas generator speed, power turbine speed and fuel flow. This non-linear behavior of the power turbine can be represented functionally [11] as

$$Q_p = Q_p(N_p, N_g, W_f) \quad .$$

This leads to the representation of Equation 11 as

$$\dot{N}_p = \frac{1}{J_p} Q_p(N_p, N_g, W_f) \quad . \tag{12}$$

By performing a Taylor series expansion about an operating point (N_{po}, N_{go}, W_{fo}) Equation 12 can be linearized

$$\Delta\dot{N}_p = \frac{1}{J_p} \left[\Delta N_p \frac{\partial Q_p(N_{po}, N_{go}, W_{fo})}{\partial N_p} + \right.$$

$$\left. \Delta N_g \frac{\partial Q_p(N_{po}, N_{go}, W_{fo})}{\partial N_g} + \Delta W_f \frac{\partial Q_p(N_{po}, N_{go}, W_{fo})}{\partial W_f} \right] \quad . \tag{13}$$

After taking the Laplace Transform, Equation 13 yields the block diagram in Figure 9.

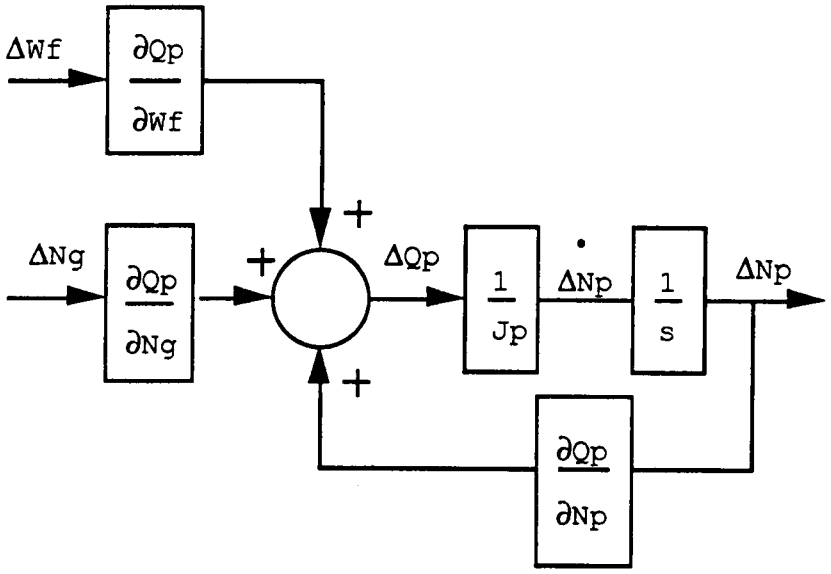

Figure 9. The power turbine model without loading effects.

ENGINE MODEL

In a free power turbine arrangement, part of the power is available as soon as fuel is burned and these hot gasses reach the power turbine. $\partial Q_p/\partial W_f$ causes an immediate power turbine enthalpy rise and is called the "fast path". There are no dynamics associated with this path; a step change in fuel flow would be felt immediately by the power turbine from this "fast path" through the engine [12].

Once the hot gases from the burning fuel cause an increase in gas generator speed, an increase in air flow to the power turbine results in an increase in the power turbine torque. This path is called the "slow path" since gas generator speed must change before there is a power output change. The "slow path" will cause a lag in the engine's

response to a full flow change. Analysis of the transfer function for $\Delta N_g(s)/\Delta W_f(s)$ shows that the change in gas generator speed, ΔN_g as a result of a fuel flow change, ΔW_f can be represented as a first order lag, where the engine time constant, T_e is inversely proportional to $\partial Q_g/\partial N_g$.

The "slow" and "fast" path through the engine were modeled in the gas generator model (refer to Figure 6), and in the power turbine model (refer to Figure 9). These figures have been combined to yield the block diagram of the engine shown in Figure 10 after block diagram manipulation. The power turbine torque due to the "fast" and "slow" path through the engine is represented by

$$\Delta Q_{pg} = \Delta N_g \frac{\partial Q_p}{\partial N_g} + \Delta W_f \frac{\partial Q_p}{\partial W_f} \quad .$$

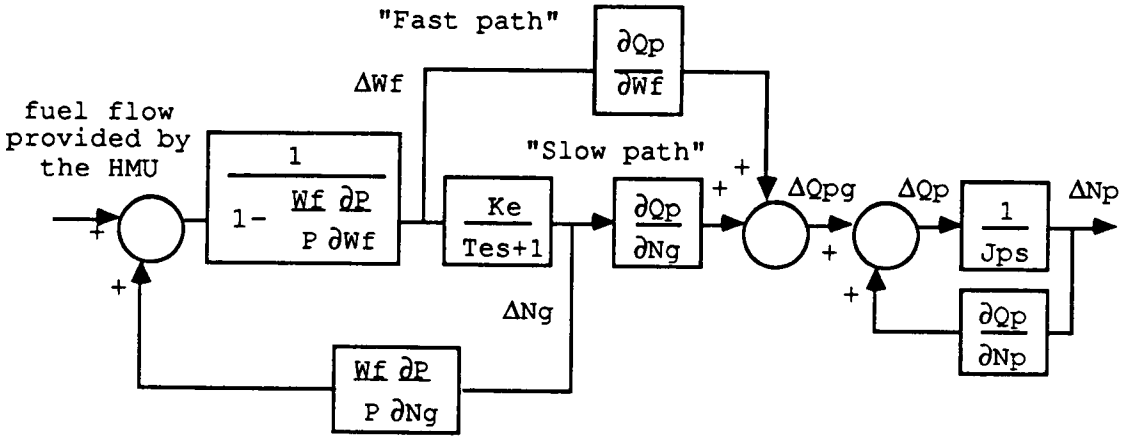

Figure 10. The engine model without loading effects.

ROTOR MODEL

During automatic rotor control, the desired rotor speed is selected by the pilot. Fuel flow is then regulated to maintain the rotor speed within the safe range for the entire helicopter operating envelope, despite load changes. The pilot adjusts the angle of the rotor blades or collective pitch, to modulate the power. An increase in the pitch of the blades will produce a drag on the rotor blades causing the engine to slow down. This behavior is referred to as transient droop. The automatic control must sense this droop and increase fuel flow so a constant rotor speed is maintained.

The main rotor inertia acts upon the fuselage to produce a twisting motion in the opposite direction. A small horizontal tail rotor is mounted vertically at the rear and on the side of the fuselage to counter the torque of the main rotor. This system is shown in Figure 11. The rotor's inertia is many times greater than the power turbine's inertia. The torsional dynamics of this system exhibits a highly underdamped characteristic [13].

Perturbation of this system can give rise to oscillations; they show up as resonant peaks on a frequency response plot where the dominant low frequency peak is due to the interaction of the power turbine with the main rotor. The interaction between the power turbine and the tail rotor creates a resonant peak at a higher frequency. The amplitude

of these peaks and the frequency at which they occur is a function of the rotor's inertia, damping, and spring constant [11].

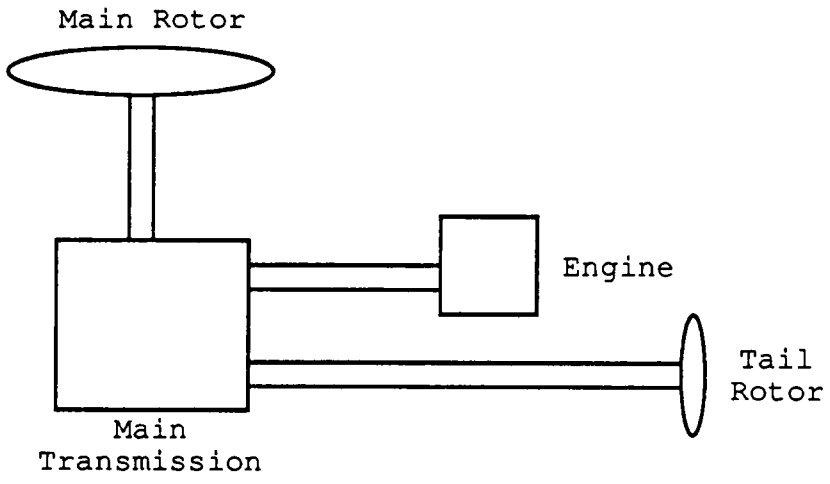

Figure 11. The rotor dynamics.

The tail rotor is not modeled since the torsional dynamics between the tail rotor and power turbine appear outside the passband of the fuel control. The behavior of the main rotor dynamics can be represented by a three mass rotor system as shown in Figure 12. This representation is recommended for helicopter manufacturers to use to supply data to the engine manufacturer for calculating the best gains and time constants for the fuel control [14].

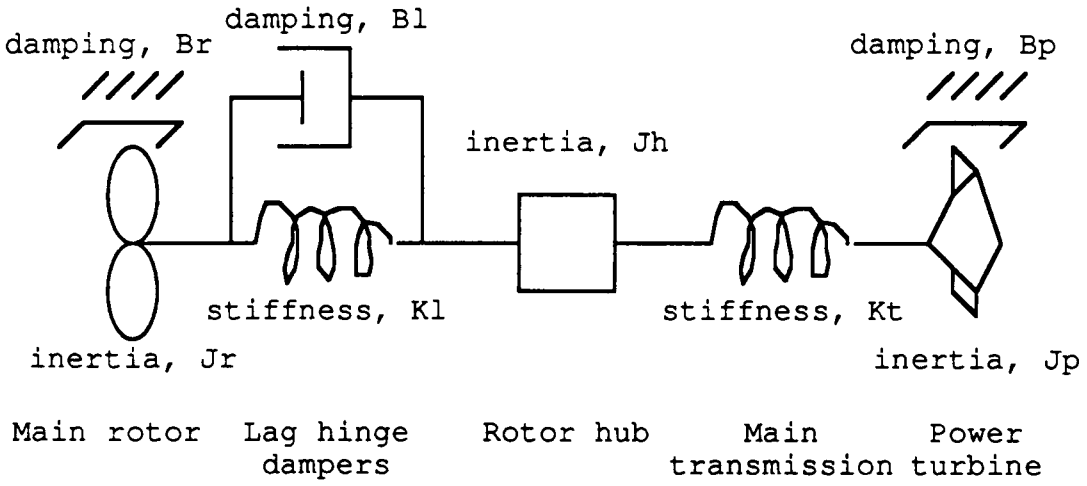

Figure 12. Three mass rotor representation.

The main rotor can be classified as one of three types: articulate, semi-rigid, and rigid. The rotor type is defined by the direction of motion and degree of movement each blade is allowed. An articulate rotor is mounted, using a vertical hinge that allows the blades to move back and forth in the rotor disc plane, and using a mechanical flapping hinge. A semi-rigid rotor only has a mechanical flapping hinge. A rigid rotor is hingeless and the mechanical flapping hinge is replaced by making portions of the rotor hub and blade flexible, to allow the blades to flap [15].

The helicopter in this study has a rigid rotor and therefore the lag hinge dampers were eliminated from the model. The other parameters were lumped to form the model shown in Figure 13. This simplification to the two mass system is used for linear stability analysis.

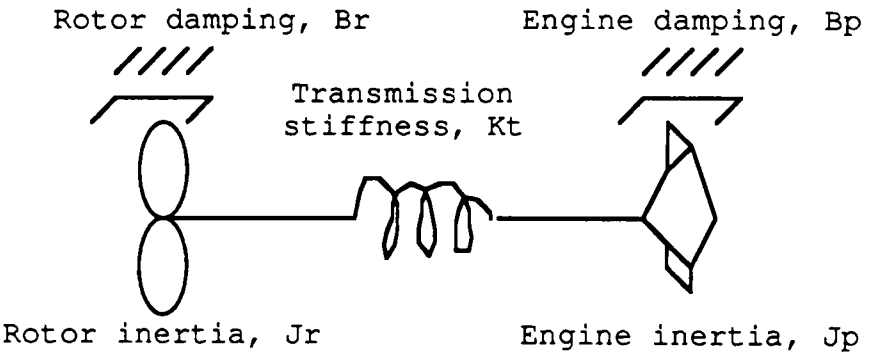

Figure 13. Two mass rotor representation.

In Figure 13, the source or power turbine has a moment of inertia, J_p and damping, B_p; the load or rotor has a moment of inertia, J_r and damping B_r. They are connected by a transmission stiffness, K_t. From Newton's law for angular motion, the sum of the torques acting on the power turbine is equal to the power turbine inertia, J_p times the angular acceleration of the power turbine or second derivative of the angular position, $\emptyset_p$ [16].

The sum of the torques include those due to the power turbine torque generated from the gas generator section, ΔQ_{pg}, the torque due to the transmission stiffness, Q_s and the torque due the damping. This relationship is

$$J_p \ddot{\emptyset}_p = \Delta Q_{pg} - K_t(\emptyset_p - \emptyset_r) - B_p \dot{\emptyset}_p \quad . \tag{14}$$

The rotor torque is described similarly,

$$J_r \ddot{\emptyset}_r = \Delta Q_d + K_t(\emptyset_p - \emptyset_r) - B_r \dot{\emptyset}_r \tag{15}$$

where ΔQ_d is the torque due to a disturbance to the rotor. This simplification ignores the internal metallic damping of the shaft itself.

The damping terms are by definition the rate of change in torque to speed, and therefore can be defined by their partial derivatives as,

$$B_p = -\partial Q_p / \partial N_p$$

$$B_r = -\partial Q_r / \partial N_r$$

where $N_p \sim \dot{\phi}_p$ and $N_r \sim \dot{\phi}_r$.

Taking the Laplace transform of Equations 14 and 15 and substituting for the damping terms,

$$J_p \, sN_p = \Delta Q_{pg} - \frac{K_t}{s} (N_p - N_r) - B_p \, N_p \qquad (16)$$

$$J_r \, sN_r = \Delta Q_d + \frac{K_t}{s} (N_p - N_r) - B_r \, N_r \, . \qquad (17)$$

The equivalent block diagram form is given in Figure 14 with the Δ representing a deviation from a steady-state operating condition [11].

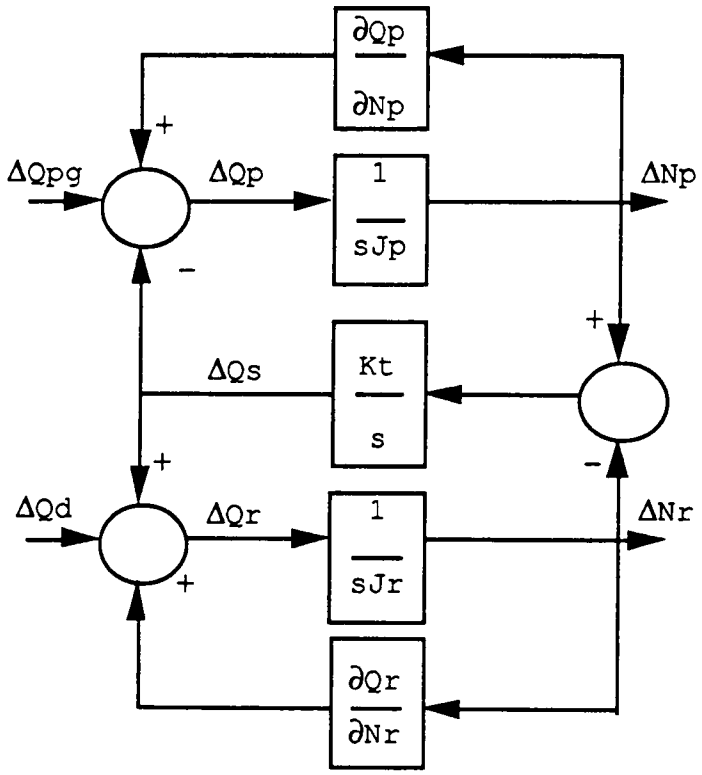

Figure 14. The rotor model.

HYDROMECHANICAL MODEL

The HMU is an electro-mechanical device that supplies fuel to the engine. It receives gas generator speed and compressor pressure from the engine and an electrical command from the electronic controller representing desired gas generator speed. The HMU consists of a gas generator governor which schedules $\Delta(W_f/P)$ as a function of the gas generator speed error. This is multiplied by the engine pressure within the HMU to generate the fuel flow supplied to the engine.

The HMU consists of the mechanics of the fuel control system and is influenced by the dynamics of the gas generator

as shown in Figure 15. It is modeled as a first order lag with a time constant.

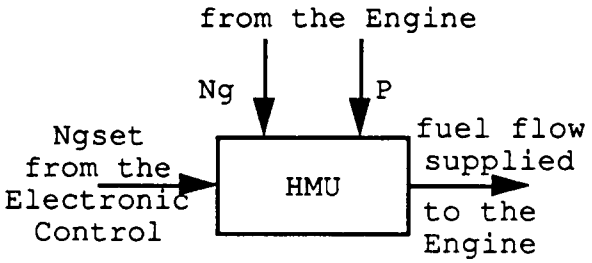

Figure 15. The HMU dynamics.

PLANT MODEL

Combining the rotor model shown in Figure 14, and the engine model shown in Figure 10, with the HMU modeled as a first order lag gives the overall block diagram of the plant as shown in Figure 16. The disturbance, ΔQ_d will be set to zero for the purpose of this control study. The speed governor maintains a constant rotor speed by setting a constant power turbine speed.

The blocks in Figure 16 are defined by the following equations:

$$G_1(s) = \frac{K_g\ K_{g\text{-}conv}\ P}{T_h s+1}\ , \qquad K_e = \frac{dN_g}{dW_f}$$

$$G_2(s) = \frac{K_e}{T_e s+1}\ , \qquad T_e = \frac{J_g}{-\frac{\partial Q_g}{\partial N_g}}$$

$$K_3(s) = \frac{1}{(1 - \frac{W_f}{P}\frac{\partial P}{\partial W_f})} \quad , \qquad G_8(s) = \frac{1}{J_p s}$$

$$K_4 = \frac{W_f}{P}\frac{\partial P}{\partial N_g} \quad , \qquad G_9(s) = \frac{K_t}{s} \quad ,$$

$$K_5 = \frac{\partial Q_p}{\partial W_f} \quad , \qquad G_{10}(s) = \frac{1}{J_r s} \quad ,$$

$$K_6 = \frac{\partial Q_p}{\partial N_g} \quad , \qquad K_{11} = \frac{\partial Q_r}{\partial N_r} \quad ,$$

$$K_7 = \frac{\partial Q_p}{\partial N_p} \quad .$$

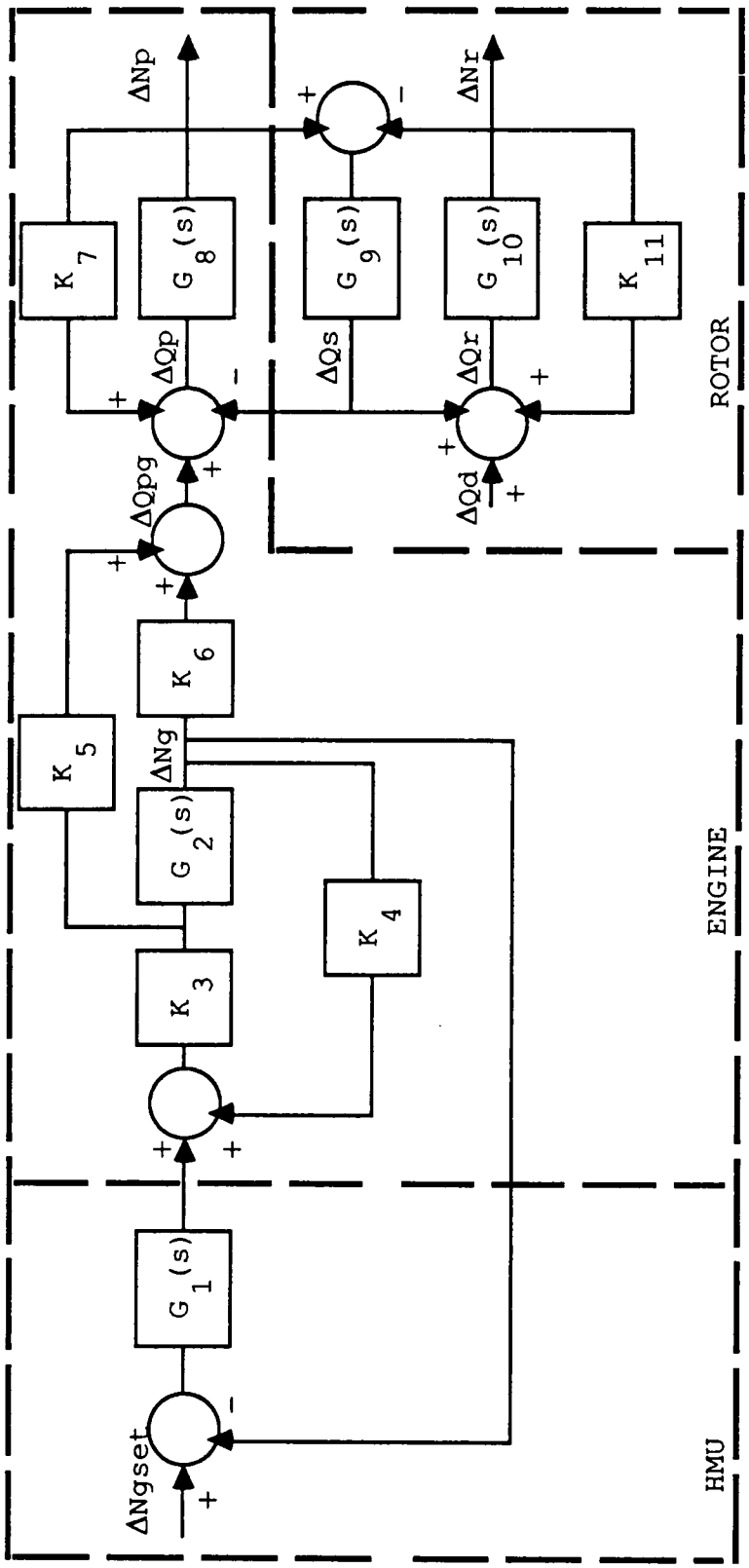

Figure 16. Block diagram of the plant.

CHAPTER III

MODEL PARAMETERS

INTRODUCTION

Linear stability analysis of the plant was performed using the data described in this section. This data was provided from two sources; Bell Helicopter provided the rotor parameters and Garrett Turbine Engine Company provided the engine parameters. The engine performance model, which was exercised to obtain the partials at each of the power points of interest is discussed. The gas generator governor gain is derived. The resultant transfer function of the plant at each power setting is shown.

ENGINE and ROTOR CONSTANTS

The engine manufacturer provided the inertia and the 100% speed for the gas generator and power turbine. Inertias, spring constants and 100% rotor speed were provided for the Bell UH-1B helicopter by Steve Killian, an employee of Bell Helicopter. These parameters were lumped, and then translated to the power turbine speed of the demonstrator engine by dividing by the gear ratio squared [17], where

$$\text{GEAR RATIO} = \frac{N_p}{N_r} = \frac{16438 \text{ rpm}}{6600 \text{ rpm}} \quad .$$

The resulting data is shown in Table 1.

Table 1. Inertias, spring constant and 100% speeds of the plant.

100% SPEED (rpm)	INERTIA (ft-lb-sec/rpm)	SPRING CONSTANT (ft-lb/rpm)
N_g = 45,306	J_g = 0.00454	K_t = 3.537
N_p = 16,438	J_p = 0.01420	
N_r = 6,600	J_r = 0.07055	

ENGINE PERFORMANCE MODEL

The engine performance model is a non-linear, computerized and thermodynamic math model which includes component maps describing each engine component, which consists of the compressor, combustor, gas generator turbine and free power turbine for this application. An engine manufacturer maintains a proprietary engine performance model on each of its engine programs. In general, all the inputs and outputs that are pertinent to the particular engine are listed, and each output variable is assumed to be a nonlinear function of all the input variables for a given steady-state operation [9].

The inputs to the performance model are ambient conditions, power setting, engine configuration, and component maps. This model combines the engine component's characteristics in the same manner as these characteristics function in the engine; each component accepts input from its adjacent components and supplies output to its adjacent

components. In this way the model simulates the steady-state performance of the engine itself [18].

The performance model was exercised to determine the partials at the four power settings of interest; the partial derivatives were calculated for the unbalanced power around the steady-state operating points corresponding to 750, 500, 250 SHP and no load, at sea level static, standard day conditions. In Chapter 2, the behavior of the gas generator and power turbine section were described as functions of W_f, N_g, and N_p. The partials were calculated from small positive and negative perturbations about a particular steady-state point. These were a deviation of 1% change in N_g, a deviation of 5% change in N_p, and a deviation of 25 pph change in W_f.

The raw data showed some inconsistencies in the data provided by the engine performance model. In general, the partial about a chosen operating point should be nearly the same in the negative and positive direction. Because this was not the case with this data the actual partials that were used in the model were derived by taking the average of the positive and negative deviation about the operating point.

At each of the power settings chosen, Q_g, Q_p, P, N_g, N_p, and W_f are calculated by the performance model. This raw data is used to calculate the partials shown in Table 2. For example, to find the partials with respect to N_g at 750 SHP, N_g is varied +-1% from its steady-state value at 750 SHP.

Table 2. Parameter variation with changes in power setting, at standard day conditions.

Parameter (units)	maximum 750 SHP	inter-mediate 500 SHP	low 250 SHP	no/load 0 SHP
P, psi	173.4	142.5	109.4	73.7
W_f, $\frac{lb}{hr}$	376.2	289.6	210.1	133.8
Q_p, ft-lb	240.5	160.6	80.7	1.0
$\frac{W_f}{P}$, $\frac{lb/hr}{psi}$	2.17	2.03	1.92	1.82
$\frac{\partial P}{\partial W_f}$, $\frac{psi}{lb/hr}$	0.0692	0.0472	0.0318	0.028
$\frac{\partial P}{\partial N_g}$, $\frac{psi}{rpm}$	0.0112	0.0119	0.01002	0.00595
$\frac{\partial Q_g}{\partial W_f}$, $\frac{ft-lb}{lb/hr}$	0.17	0.1946	0.1988	0.2066
$\frac{\partial Q_g}{\partial N_g}$, $\frac{ft-lb}{rpm}$	-0.00814	-0.00776	-0.00596	-0.00458
$\frac{\partial Q_p}{\partial N_g}$, $\frac{ft-lb}{rpm}$	0.02368	0.02216	0.01445	0.00676
$\frac{\partial Q_p}{\partial W_f}$, $\frac{ft-lb}{rpm}$	0.3798	0.3116	0.3808	0.4834
$\frac{\partial Q_p}{\partial N_p}$, $\frac{ft-lb}{rpm}$	-0.01119	-0.00991	-0.01228	-0.01159
$\frac{\partial Q_r}{\partial N_r}$, $\frac{ft-lb}{rpm}$	-0.02926	-0.01954	-0.00982	-0.00
$\frac{dN_g}{dW_f}$, $\frac{rpm}{lb/hr}$	20.88452	25.07732	33.3557	45.1092

When N_g is perturbed from its steady-state operating point at 750 SHP, each of the other parameters will vary from their steady-state operating point by some delta, Δ. If the partial

of interest is $\partial Q_g/\partial N_g$, then the ΔQ_g and ΔN_g from the performance model is used, where

$$\frac{\Delta Q_g}{\Delta N_g} \rightarrow \frac{\partial Q_g}{\partial N_g} \quad .$$

The results of these calculations are shown in Table 2. All parameters in Table 2 are obtained by exercising the performance model, except $\partial Q_r/\partial N_r$ and dN_g/dW_f. At each power point, dN_g/dW_f was calculated from,

$$\frac{dN_g}{dW_f} = \frac{\partial Q_g/\partial W_f}{-\partial Q_g/\partial N_g} \quad .$$

Calculation of $\partial Q_r/\partial N_r$ is determined by using Equation 18; at a fixed collective pitch, the torque on the rotor is proportional to the rotor speed squared, since centrifugal force is a function of the rotating speed squared

$$Q_r = K\ N_r^2 \quad . \tag{18}$$

Thus,

$$\frac{\partial Q_r}{\partial N_r} = 2\ K\ N_r \tag{19}$$

$$= 2\ \frac{Q_r}{N_r} \quad . \tag{20}$$

Since the power turbine and the rotor are connected on the same shaft,

$$Q_r N_r = Q_p N_p \quad . \tag{21}$$

Solving for Q_r and using this in Equation 20 gives,

$$\frac{\partial Q_r}{\partial N_r} = 2 \frac{Q_p N_p}{N_r^2} \quad . \tag{22}$$

The rotor and power turbine are connected by a transmission gear system and therefore the rotor damping is translated to the power turbine speed by dividing by the gear ratio squared

$$\frac{\partial Q_r}{\partial N_r} = 2 \frac{Q_p}{N_p} \quad . \tag{23}$$

The damping of the power turbine will have a negative value as given by the performance model and shown in Figure 8. The rotor damping also has a negative slope since it acts to stabilize the helicopter by producing a moment opposite to the moment which produces a tilting force [19].

At no load condition or zero SHP, the $\partial Q_r/\partial N_r$ is zero and the spring constant is set to zero. The transfer function for the power turbine torque generated by the gas generator section to the power turbine speed is

$$\frac{\Delta N_p(s)}{\Delta Q_{pg}(s)} = \frac{\frac{1}{J_p}}{s - \frac{\frac{\partial Q_p}{\partial N_p}}{J_p}} \quad . \tag{24}$$

For the coupled rotor case, this transfer function is

$$\frac{\Delta N_p(s)}{\Delta Q_{pg}(s)} = \frac{\frac{1}{J_p}\left(s^2 - \frac{\frac{\partial Q_r}{\partial N_r}}{Jr}s + \frac{K_t}{J_r}\right)}{s^3-\left(\frac{1}{J_r}\frac{\partial Q_r}{\partial N_r}+\frac{1}{J_p}\frac{\partial Q_p}{\partial N_p}\right)s^2+\left(\frac{K_t}{J_r}+\frac{K_t}{J_p}+\frac{1}{J_pJ_r}\frac{\partial Q_p}{\partial N_p}\frac{\partial Q_r}{\partial N_r}\right)s-\frac{K_t}{J_pJ_r}\left(\frac{\partial Q_p}{\partial N_p}+\frac{\partial Q_r}{\partial N_r}\right)} \quad (25)$$

Equation 25 can be reduced to Equation 24 by setting K_t and $\partial Q_r/\partial N_r$ equal to zero.

Using MATLAB, the frequency and step response plots for the coupled rotor case at no load condition were made with a value of 0.002 for the $\partial Q_r/\partial N_r$ which is equivalent to about 40 SHP. This substitution for the zero SHP, coupled rotor case is realistic, since the rotor being coupled and the shaft horsepower being equal to zero is not physically realizable.

GAS GENERATOR GOVERNOR DESIGN

The gain of the HMU, K_g was set to 0.7 and can be calculated from the time constant in the transfer function of actual gas generator speed to gas generator setpoint. The transfer function was found from Figure 16 as

$$\frac{\Delta N_g(s)}{\Delta N_{gset}(s)} = \frac{K_3\ G_1(s)\ G_2(s)}{1 - K_3\ K_4\ G_2(s) + K_3\ G_1(s)\ G_2(s)} . \quad (26)$$

Substituting in the time constants, gains, and partial derivatives, the transfer function is

$$\frac{\Delta N_g(s)}{\Delta N_{gset}(s)} =$$

$$\frac{(K_g\ K_{g\text{-}conv}\ P\ K_{NW})}{(T_eT_hs^2 + [T_e+T_h(1+K_{NW}K_{GW})]s + [1+K_gK_{g\text{-}conv}\ P\ K_{NW}+K_{NW}K_{GW}])}$$

where,

$$K_{NW} = \frac{K_e}{(1 - \frac{W_f}{P}\frac{\partial P}{\partial W_f})} \tag{27}$$

$$K_{GW} = \frac{W_f}{P}\frac{\partial P}{\partial N_g} \tag{28}$$

$$K_e = \frac{dN_g}{dW_f}, \qquad T_e = \frac{J_g}{\frac{-\partial Q_g}{\partial N_g}}.$$

T_h represents the HMU time constant of 0.045 seconds.

K_{NW} represents the change in gas generator speed due to fuel flow as modified by the change in compressor discharge pressure.

K_e represents the basic engine or gas generator gain in the transfer function of $\frac{\Delta N_g(s)}{\Delta W_f(s)}$.

T_e represents the basic engine or gas generator time constant in the transfer function of $\frac{\Delta N_g(s)}{\Delta W_f(s)}$.

$K_{g\text{-}conv}$ has units of $\frac{100\%Ng}{45306rpm}$.

PLANT TRANSFER FUNCTION

The open loop transfer function, of the plant is given by Equation 29

$$\frac{\Delta N_p(s)}{\Delta N_{gset}(s)} = \frac{\Delta N_g(s)}{\Delta N_{gset}(s)} \quad \frac{\Delta Q_{pq}(s)}{\Delta N_g(s)} \quad \frac{\Delta N_p(s)}{\Delta Q_{pq}(s)} \; . \qquad (29)$$

At 750 SHP:

$$\frac{\Delta N_p(s)}{\Delta N_{gset}(s)} = \frac{514\ (s + 4)\ (s^2 + 0.4s + 50)}{(s^2 + 23s + 272)\ (s^3 + s^2 + 300s + 142)}$$

At 500 SHP:

$$\frac{\Delta N_p(s)}{\Delta N_{gset}(s)} = \frac{318\ (s + 5)\ (s^2 + 0.3s + 50)}{(s^2 + 22.7s + 241)\ (s^3 + s^2 + 300s + 104)}$$

At 250 SHP:

$$\frac{\Delta N_p(s)}{\Delta N_{gset}(s)} = \frac{288\ (s + 3)\ (s^2 + 0.3s + 50)}{(s^2 + 22.6s + 181)\ (s^3 + s^2 + 300s + 78)}$$

At 0 SHP:

$$\frac{\Delta N_p(s)}{\Delta N_{gset}(s)} = \frac{244\ (s + 2)\ (s^2 + 50)}{(s^2 + 23s + 130)\ (s^3 + 0.8s^2 + 300s + 41)}$$

At 0 SHP and rotor decoupled:

$$\frac{\Delta N_p(s)}{\Delta N_{gset}(s)} = \frac{244\ (s + 2)}{(s^2 + 23s + 130)\ (s + 0.8)}$$

The transfer function of the plant is analyzed in the next two sections to determine its frequency response and transient response characteristics prior to designing the controller compensation.

CHAPTER IV

THE ANALYSIS

INTRODUCTION

The two major effects that can cause instability of the engine and rotor system are discussed in this chapter. Then design goals are developed which maintain stability as well as provide good steady-state and transient performance of the system. Each type of controller compensation that is used to meet the design goals is described along with its effect on the plant. The analysis program, MATLAB is used to obtain the frequency and step response plots.

TORSIONAL RESONANCE

The torsional resonant amplification at the coupled rotor and power turbine natural frequency can be predicted accurately with linear analysis [20]. The torsional frequency, ω_r is shown in the Bode plot of the transfer function of the rotor coupled to the power turbine, $\Delta N_p/\Delta Q_{pg}$. It is predicted by this model to occur around 17.3 rad/sec as shown in Figure 17. At this critical frequency, torsional resonance is caused by the coupled response of the rotor to the engine. Amplification of the resonant peaks of the power turbine and rotor system is the major destabilizing effect

that can drive the system unstable and therefore must be attenuated by the speed governor.

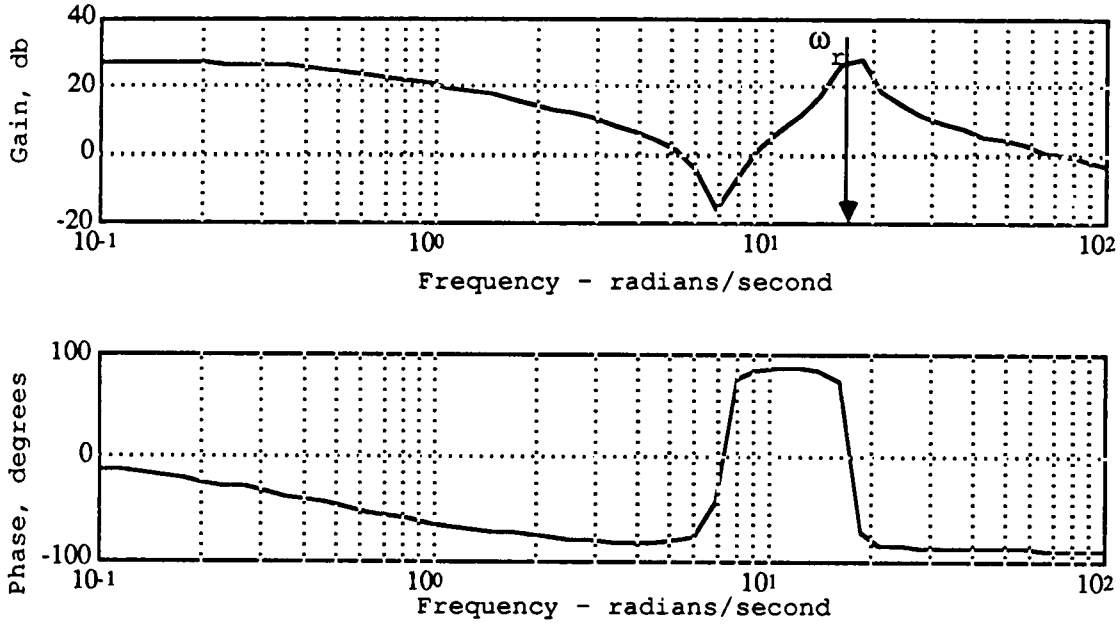

Figure 17. Frequency response of $\frac{\Delta N_p}{\Delta Q_{pg}}$ at 750 SHP.

AUTOROTATION

During a combat situation it may become necessary to perform a quick turn maneuver causing the rotor to suddenly unload. As the rotor decouples from the power turbine there is an increase in the system loop gain. This appears at the frequency at which the system tends to oscillate when behaving as a feedback system with a simple non-resonant load.

This destabilizing effect is observable on the cockpit gauge when the needles showing torque and speed move in opposite directions; this condition is referred to as "split-needles". When this occurs, the air drives the rotor in what is called autorotation and the rotor decouples from the engine. It is not accurately predicted by linear analysis. To study the effects of rotor decoupling, plots will be made for the decoupled rotor case and the coupled rotor case, at no load (or zero SHP).

DESIGN GOALS

Controller design goals are chosen to meet transient response, steady-state accuracy and stability requirements. The controller must provide: accurate control (governing) of the rotor speed over the load ranges from zero to maximum SHP, stable governing of the high inertia rotor system when coupled to the low inertia power turbine over the full range and without supporting shaft drive system torsional excitations, and stable governing of the low inertia power turbine when decoupled from the rotor system. Design goals were chosen to provide stability without compromising transient performance.

In a military helicopter, where quick maneuvers are required, the transient performance of the speed governor is critical. The system response should be as quick as possible while maintaining system stability. Minimizing the steady-

state error will increase the performance of the control. The degree of steady-state accuracy, along with good transient response determines how well the design reduces the pilot's workload, by relieving the pilot of continuously monitoring the operation and performance of the engines during critical flight maneuvering. In a combat situation this is important since the pilot's attention is split between maneuvering the helicopter and the firing of weapons. Since the pilot may not be able to respond fast enough, the speed and accuracy of the control's response is critical, such as when an engine malfunctions causing a loss of power.

A measure of the transient performance is the bandwidth which is equal to the gain crossover frequency at zero decibels. The higher the bandwidth, the more effective the governor. If the bandwidth is too low, this will result in a slow and inaccurate system. The gain and phase margin provide a measure of stability. The gain margin is a measure of the torsional stability and it is equal to the negative value of the dB gain at the phase crossover frequency. An increase in the loop gain to improve the bandwidth will decrease the gain margin and increase the gain at the torsional frequency. The phase margin is equal to 180° plus the phase at the gain crossover frequency. The goal is to maintain an acceptable gain and phase margin, with the highest bandwidth or gain crossover frequency attainable.

Typical design criteria for a control system may specify a gain margin between 2 dB and 10 dB and a phase margin between 30° and 60° [21]. A phase margin in excess of 45°, insures stability for a system with oscillatory tendencies, such as the helicopter engine and rotor system [20]. The open-loop stability analysis of the coupled rotor (shown in Figure 17) shows the critical factor to be the peak in the gain curve. The magnitude of this peak is what determines the torsional stability of the rotor coupled to the engine. Attenuation of the gain at this critical frequency to at least -6 dB is desirable. An attenuation of 6 dB normally limits the bandwidth of most rotor system controllers to 3 rad/sec [11]. This is because any compensation that tends to increase the bandwidth will also increase the resonant peak and decrease the gain margin. These design goals are summarized in Table 3.

The goal is to maximize bandwidth while minimizing the steady-state error, and while maintaining the stability requirements. Using Bode analysis and control methodology, the gain margin and phase margin at the phase and gain crossover frequencies, respectively were evaluated. In addition the two effects which cause instability in this system - which occur at the torsional frequency, and upon rotor decoupling - are studied. To study the torsional stability, the gain was evaluated at the torsional frequency.

To study the effect of the rotor decoupling, plots were made of the coupled and decoupled rotor at zero shaft horsepower.

Table 3. Design goals for the engine and rotor system.

Stability	
Gm, Gain Margin	= 6 dB
Pm, Phase Margin	= 45°
Gr, Gain @ resonant peak	<= -6 dB
Transient Performance	
BW, Bandwidth or zero decibel gain crossover	= 3 rad/sec
Steady-state Accuracy	
SS err, Steady state error	< 15%

MATLAB

The linear model was entered in block diagram form using a program called MATLAB. Subroutines were set-up which defined the controller gains and model parameters. This allowed model parameters to be changed easily for a given run. All Bode and step response plots were made using MATLAB.

CHAPTER V

CONTROLLER DESIGN

INTRODUCTION

Stability and transient response analysis was based on a linear representation of the engine, rotor system and HMU, hereafter referred to as the plant. The piecewise linear model was studied at four power points; maximum power (750 SHP), intermediate power (500 SHP), and low power (250 SHP) for the coupled rotor (CR), and no load (zero SHP) for the coupled and decoupled rotor (DR).

This chapter presents the results of applying compensation to the plant. Three types of compensation are considered: 1) proportional 2) first order lag 3) second order notch filter. The effect of each type of compensation on the plant is discussed. Compensation was selected for the 750 SHP case first. The chosen compensator was then applied at each of the four power levels. Both frequency response and time response analysis was performed to show that specifications had been met.

PLANT ANALYSIS

First the plant was analyzed without compensation. Evaluation of the coupled rotor case in Figure 18 showed similar results at each power level. The plant with the rotor

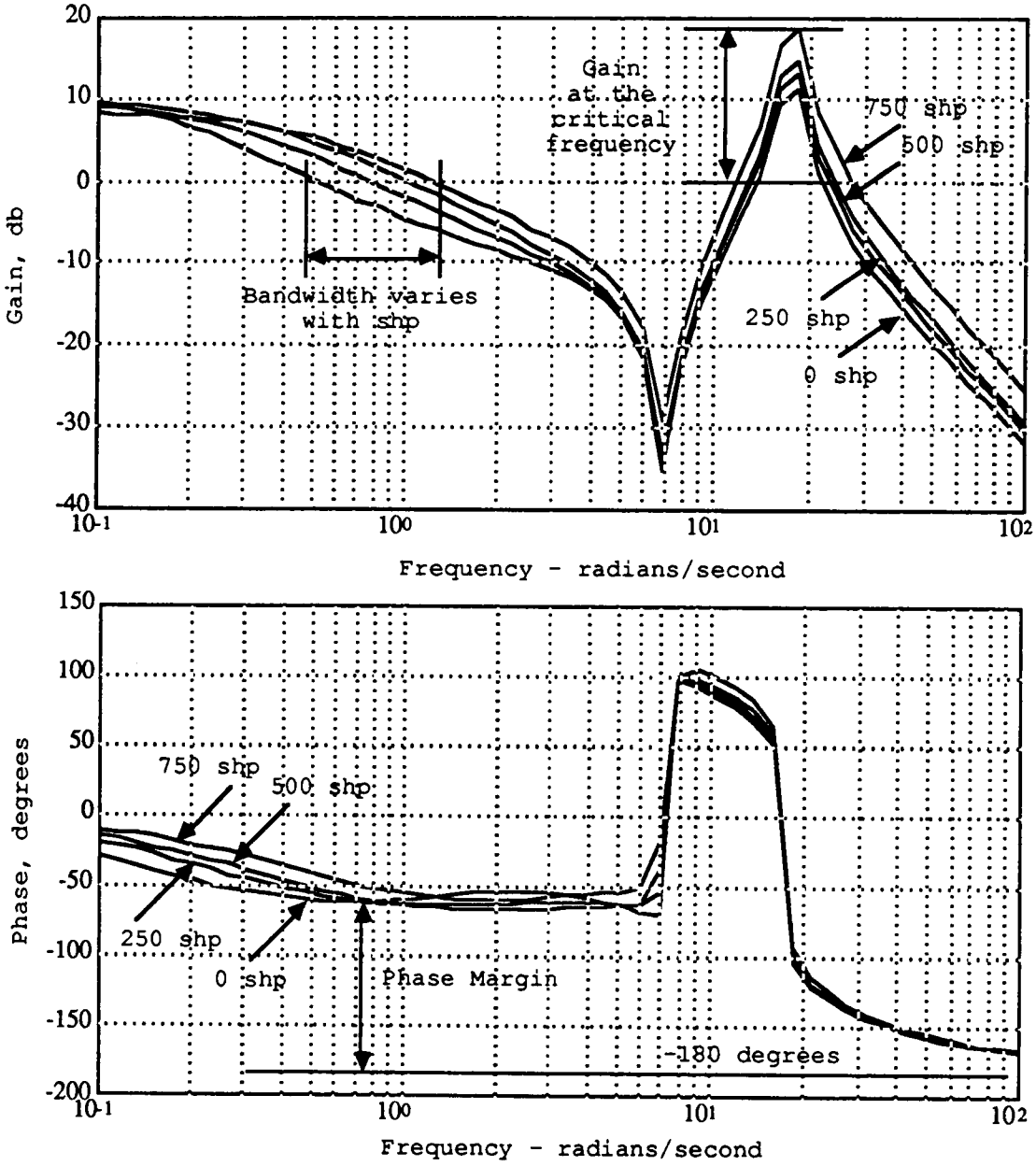

Figure 18. Open-loop frequency response of the plant with the rotor coupled, at each power level.

coupled exhibits a high gain peak at the torsional frequency (ω_r) of 17.3 rad/sec. The gain at the critical frequency (GR)

increased as the power level was increased; worst case results were at 750 SHP, with a resonant peak of 19 dB.

Increasing the engine power increases the speed loop gain, improving transient performance; the resulting bandwidth (BW) was 0.52 rad/sec at zero SHP and 1.2 rad/sec at 750 SHP. The bandwidth of 1.2 rad/sec indicates slow responsiveness to pilot commands. The phase margin (PM) of approximately 120° varied little with power level. At all parametric conditions, the phase did not cross -180°, therefore the gain margin (GM) is undefined (U/D). Since the system does not meet the specifications, a compensator was required.

The rotor's torsional resonance limits the governor response, therefore the system loop gain and resulting bandwidth is much higher with the rotor decoupled as shown in Figure 19. Hence the transient response is much faster for the decoupled rotor case than for the coupled rotor case. The decoupled rotor case exhibits sufficient phase margin and a high bandwidth, but the steady-state error (ss-err) of 21% is unacceptable. The steady-state error was found by letting ΔN_{gset} be a unit step function and plotting the closed-loop step response at ΔN_p.

A power turbine speed request step change was input into the uncompensated model at each power level and showed the steady-state error to range from 21% to 27%. With increasing

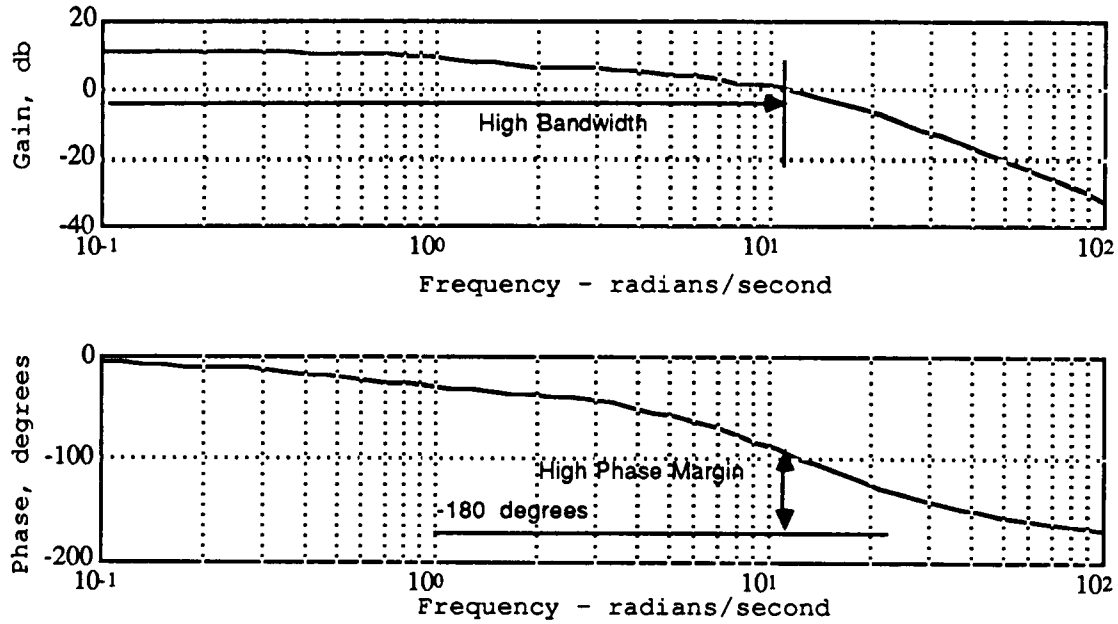

Figure 19. Open-loop frequency response of the plant with the rotor decoupled.

power level, the steady-state error increases as shown in Table 4. The parametric conditions at 750 SHP yields the highest steady-state error. A step response for this

Table 4. Steady-state error of the uncompensated plant.

configuration (config)	shaft horsepower (SHP)	steady-state error (ss-err)
DR	0	21%
CR	0	21%
CR	250	24%
CR	500	25%
CR	750	27%

condition is shown in Figure 20. The resulting torsional instability is caused by the high positive gain at the critical frequency.

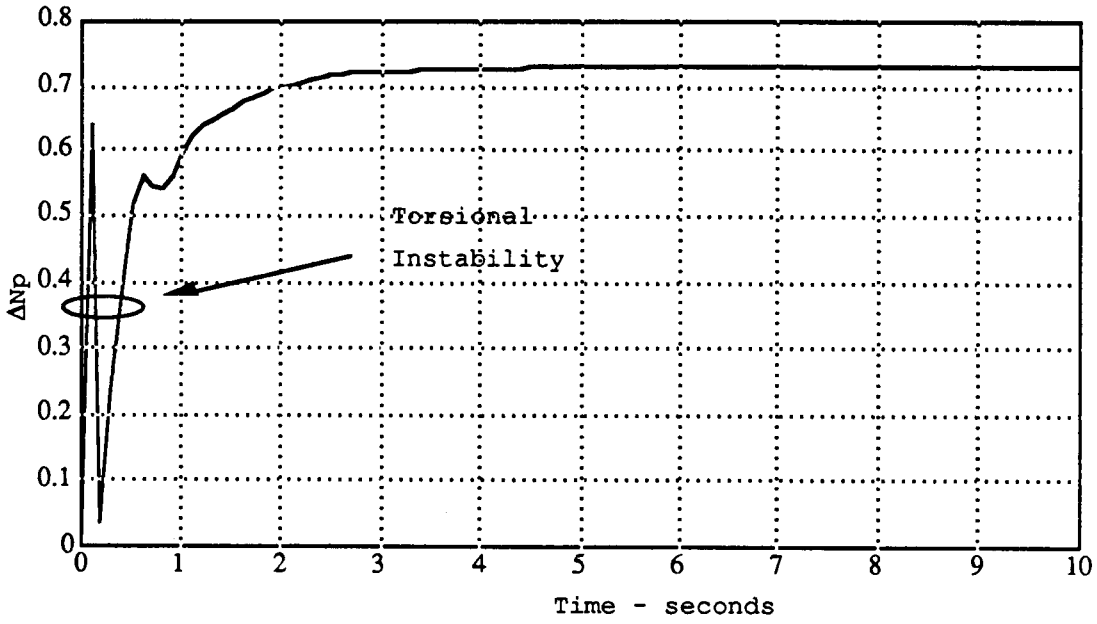

Figure 20. Closed-loop step response of the plant at 750 SHP.

The compensator will be designed for 750 SHP. Applying this compensation to the other power levels should produce better results, since the steady-state error and resonant peak decrease as the power level is decreased. The bandwidth also decreases as the power level is decreased and therefore the gain and time constants will be chosen to yield a high bandwidth at 750 SHP, to minimize the degradation in performance when applied to the lower power levels.

The best controller gains and time constants chosen for the coupled rotor plant will also be applied to the decoupled rotor plant. If these are not acceptable, they will be adjusted to meet design goals. The behavior of the plant without compensation is summarized in Table 5.

TABLE 5. Summary of the behavior of the uncompensated plant.

config	SHP	GM (dB)	PM (degrees)	BW (rad/sec)	GR (rad/sec)
DR	0	U/D	+ 88	11.12	N/A
CR	0	U/D	+120	0.52	11
CR	250	U/D	+118	0.78	13
CR	500	U/D	+116	1.02	16
CR	750	U/D	+123	1.22	19

COMPENSATOR DESIGN

To meet the specifications, the effect of adding proportional, phase lag and standard notch filtering was studied. Adjustments to the controller gains or time constants for each type of compensation were made to shape the Bode diagram to meet the design goals. Addition of compensation to the plant shown in Figure 16 where $G_{12}(s) = K_{p\text{-}conv}$ is shown in Figure 21 with,

$$G_{12}(s) = \left[\frac{K_p\, K_{p\text{-}conv}}{T_p s+1}\right] \left[\frac{s^2 + 2\zeta_{lag}\, \omega_n\, s + \omega_n{}^2}{s^2 + 2\zeta_{lead}\, \omega_n\, s + \omega_n{}^2}\right] \quad . \qquad (30)$$

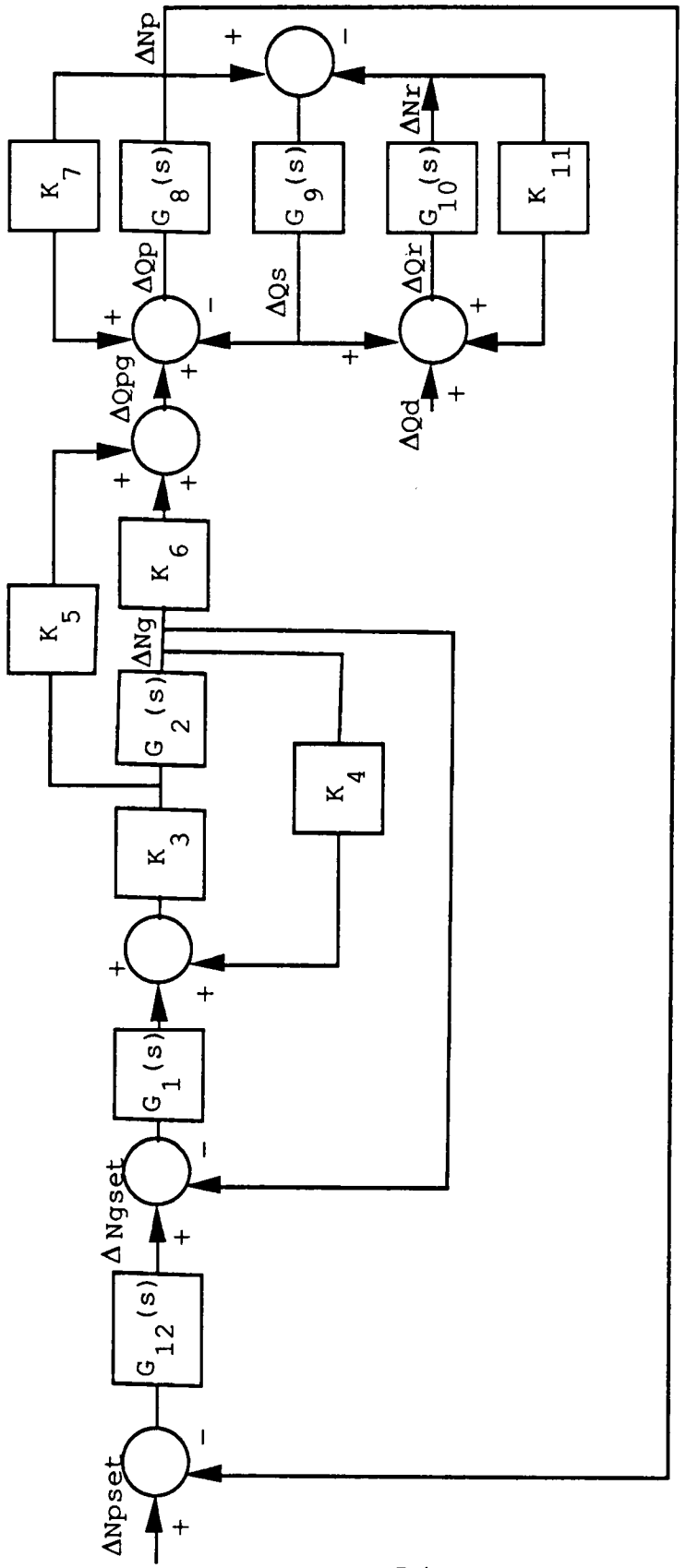

Figure 21. Block diagram of the system.

The use of proportional in cascade with the plant will increase the gain of the system at all frequencies. By increasing the system bandwidth, the engine response is quicker and handling qualities are improved. However, torsional stability complicates the compensator design since the flexibility of the rotor shaft and dynamics of a free power turbine make meeting stability requirements difficult. An increase in gain to meet the transient response amplifies the rotor instability. Therefore proportional control only is unacceptable.

The use of phase lag in cascade with the plant will attenuate the gain at higher frequencies and therefore, decrease the resonant peak. The bandwidth would also be reduced causing a tendency towards slow response. The phase margin would be reduced as a result of the phase shift at the gain crossover. Reduction to less than 45° will cause underdamped low frequency fluctuations at the gain crossover.

The use of a phase lag in cascade with the plant will meet the stability requirements by compromising engine performance. If the bandwidth is too low, the control will have a slow response to the pilot's commands resulting in longer stabilization times following a disturbance. Taken to the extreme, too slow a response can cause the feedback signal to add to the reference signal and produce an unstable system. Therefore, phase lag by itself was considered

unacceptable. Adjustments of the time constant and the system gain were evaluated by adding $\frac{K_p}{T_p s+1}$, in series with the plant.

The time constant for the phase lag (T_p) was sized to meet the following criteria:

1. Make the pole greater than the desired bandwidth, to minimize attenuation at low frequencies and thereby minimize the effect on the bandwidth.

2. Make the pole less than the critical frequency of 17.3 rad/sec, to maximize the effect on attenuating the resonant peak. The smaller the pole, the greater the attenuation at the critical frequency.

3. Make the pole high enough that the incurred phase lag does not create an unacceptable phase margin.

The second and third criteria must be met to ensure stability. K_p can then be added to meet the bandwidth requirements.

To meet the design goal of a gain of -6 dB at the critical frequency, the resonant peak must be attenuated by 25 dB. A phase lag with time constant of 0.8 sec will be down 20 dB by 10 times the pole at 1.25 rad/sec as shown in Figure 22. A time constant of 0.8 sec has a gain of about -22.8 dB and phase angle of 86° at the critical frequency of 17.3 rad/sec.

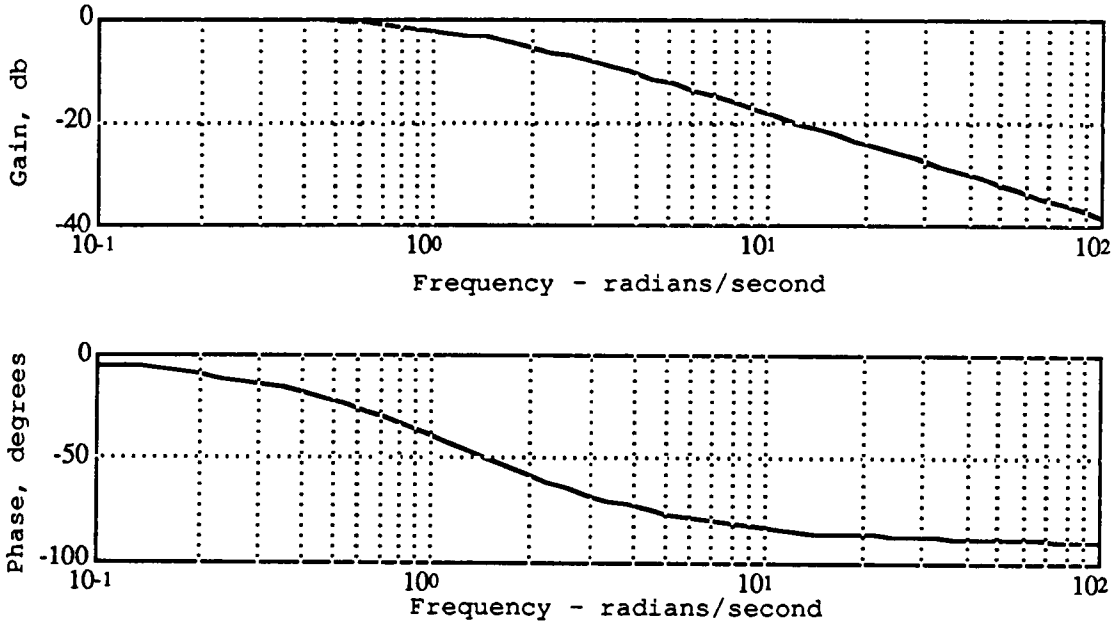

Figure 22. Frequency response of $\frac{1}{T_p s + 1}$ with phase lag of 0.8 sec.

When added to the plant as shown in Figure 23, this resulted in a gain margin of 5.2 dB at the phase crossover of 18.6 rad/sec and a phase margin of 89° at the gain crossover of 0.93 rad/sec. The incurred phase lag has not adversely affected the system since there is still plenty of phase margin. The resonant peak has been attenuated only to -2.2 dB producing oscillations in the closed-loop step response shown

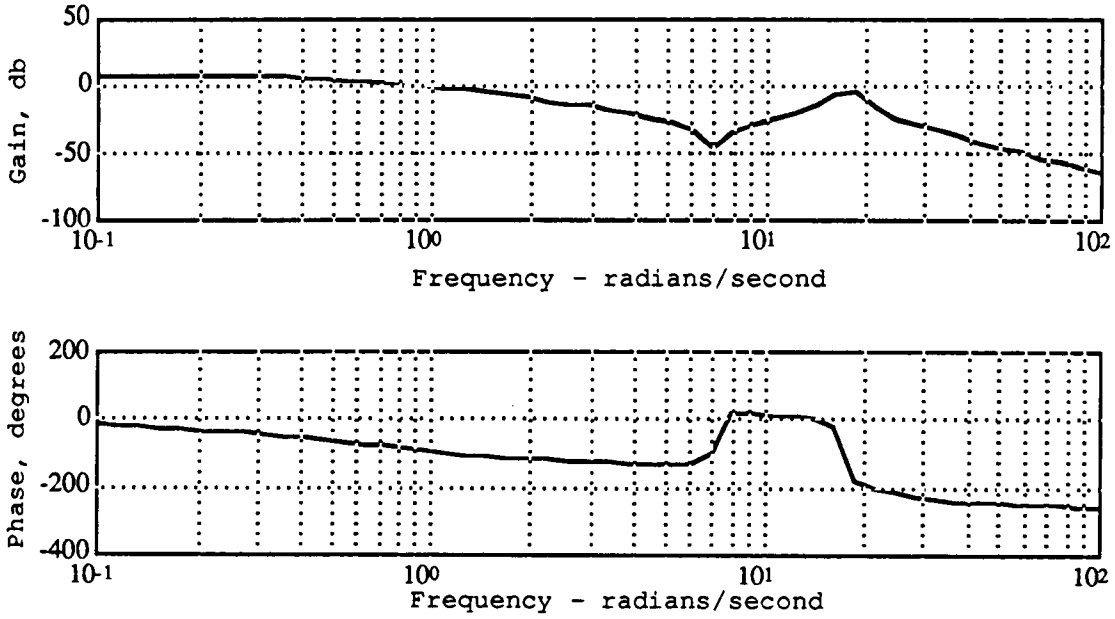

Figure 23. Open-loop frequency response of the system at 750 SHP with a phase lag of 0.8 sec.

in Figure 24. The bandwidth of 0.93 rad/sec produces a slow and inaccurate system with a steady-state error of 27%.

An increase in K_p to increase the bandwidth would also increase the resonant peak and drive the system unstable. Using proportional and phase lag in series with the plant will not yield a stable system without producing a slow system response and high steady-state error. Therefore the use of a notch filter was investigated to allow using proportional to design for bandwidth at the low frequency and using the phase lag and the notch to attenuate the gain at the critical frequency.

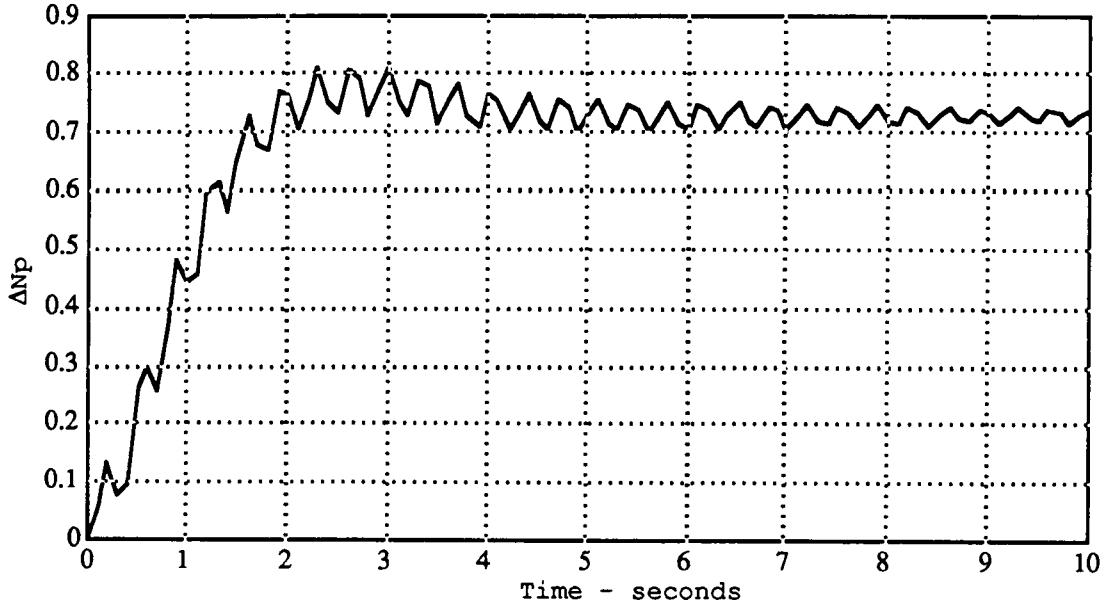

Figure 24. Closed-loop step response of the system at 750 SHP with a phase lag of 0.8 sec.

A secondary purpose of the control lag was to add tolerance or robustness for any inaccuracies in the model. Because of modeling errors associated with the rotor system, the torsional oscillations may be worse than predicted by the model (i.e. the resonant frequency may occur at a different frequency, and the resonant peak may be higher than predicted by the model). If the resonant frequency predicted by the model is not correct, the addition of the lag adds a measure of margin to the design, by attenuating the gain at the higher frequencies.

Since the notch can be designed to provide enough attenuation at the resonant peak, a smaller time constant of 0.25 sec for the cascade phase lag was chosen to produce a

higher bandwidth and minimize the effect on the phase margin. The effect of this phase lag on the plant is shown in Figure 25.

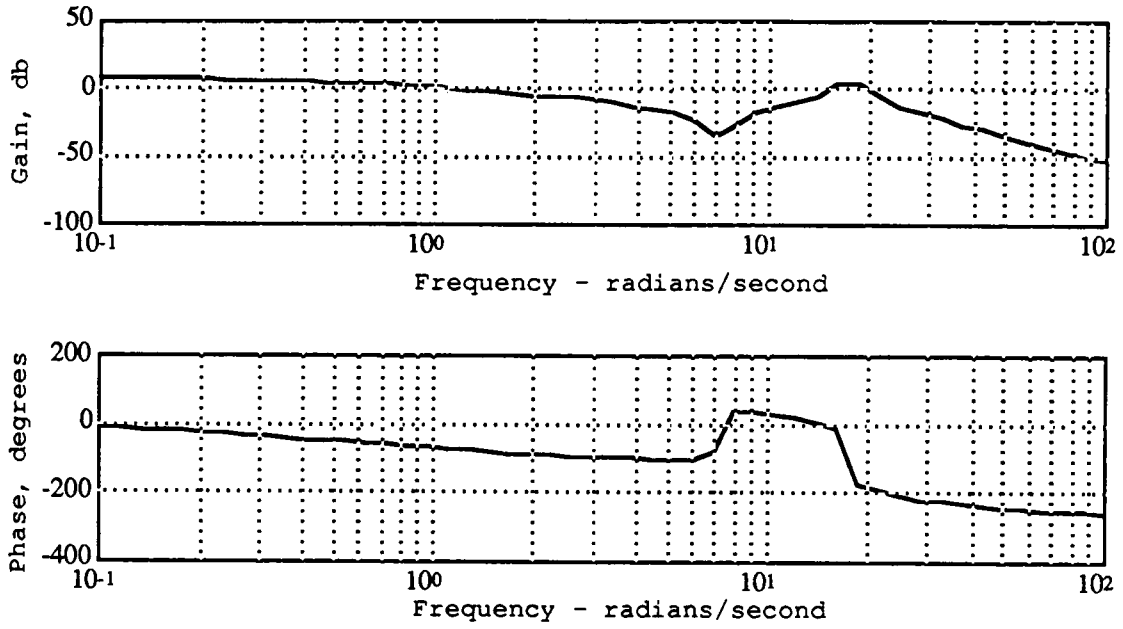

Figure 25. Open-loop frequency response of the system at 750 SHP with a phase lag of 0.25 sec.

The addition of a 0.25 sec phase lag resulted in a positive gain at the resonant peak, resulting in a gain margin of -2.01 dB at 19.57 rad/sec, producing an unstable system. The gain crossover of 1.16 rad/sec is not enough bandwidth for good transient response. The phase margin of 106.86° is sufficient.

To reach a desired bandwidth of 3 rad/sec, the gain must be increased by 9 dB at 2 rad/sec. The results of adding proportional, with a K_p of 2.85 is shown in Figure 26. The bandwidth of 3.03 rad/sec has been achieved at the expense of further increasing the resonant peak resulting in a gain margin of -11.11 dB at 19.57 rad/sec.

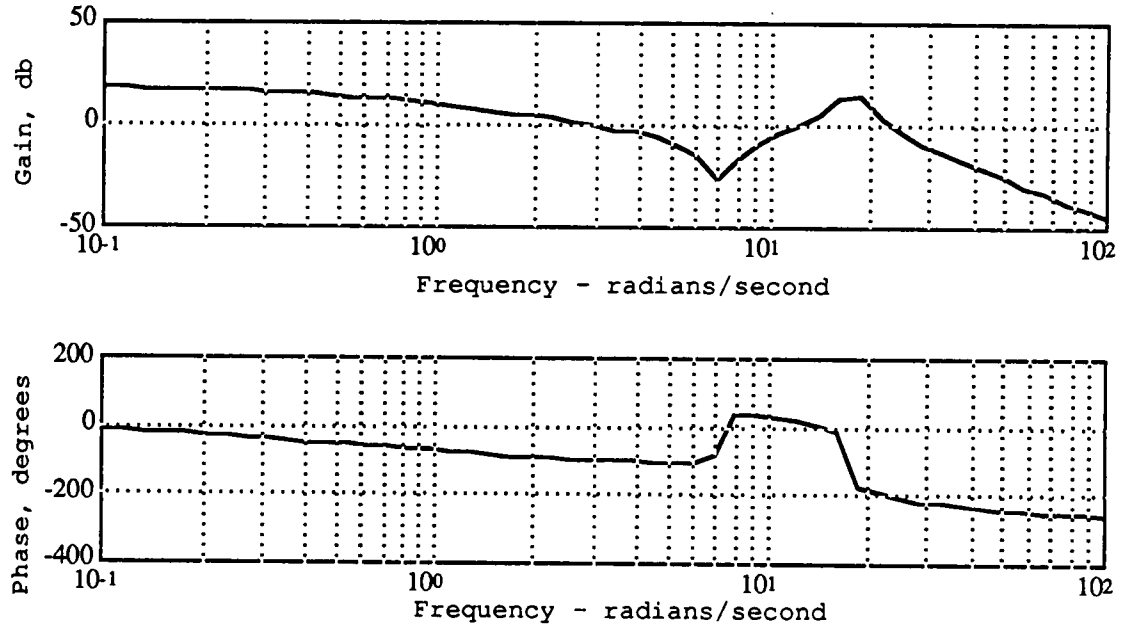

Figure 26. Open-loop frequency response of the system at 750 SHP with T_p=0.25 and K_p=2.85.

A notch filter was designed to attenuate the open-loop gain at the resonant frequency. The use of the notch attenuates the gain at the torsional resonance without introducing excessive phase shift at the gain crossover

frequency. A 2.75 Hz notch was designed with the following considerations. The lead function was in the form of,

$$\frac{1}{\frac{s^2}{\omega_n^2} + \frac{2\zeta_{lead}}{\omega_n} s + 1} = \frac{\omega_n^2}{s^2 + 2\zeta_{lead}\omega_n s + \omega_n^2} \qquad (31)$$

and the lag function was in the form of,

$$\frac{1}{\frac{s^2}{\omega_n^2} + \frac{2\zeta_{lag}}{\omega_n} s + 1} = \frac{\omega_n^2}{s^2 + 2\zeta_{lag}\omega_n s + \omega_n^2} \; . \qquad (32)$$

When combined the transfer function for the notch is,

$$\frac{\frac{s^2}{\omega_n^2} + \frac{2\zeta_{lag}}{\omega_n} s + 1}{\frac{s^2}{\omega_n^2} + \frac{2\zeta_{lead}}{\omega_n} s + 1} = \frac{s^2 + 2\zeta_{lag}\,\omega_n\, s + \omega_n^2}{s^2 + 2\zeta_{lead}\,\omega_n\, s + \omega_n^2} \; . \qquad (33)$$

Lag compensation results in a large increase in gain. If this function is inverted, the gain and phase angle are the same, but with a change in sign. For lag compensation, ζ_{lag} is less than 1.0 and the smaller ζ_{lag}, the bigger the peak in the gain curve. Since the quadratic factor appears in the numerator of Equation 33, the notch will attenuate the resonant peak. To compensate for the torsional peak, ζ_{lag} will be minimized.

The lead compensation was designed to minimize the introduction of phase shift. The best results were achieved with ζ_{lead} ten times greater than ζ_{lag}. For frequencies much more or less than ω_n, the gain of these two functions cancel and have no affect on the system and therefore no impact on the bandwidth. The incurred phase shift at the gain crossover frequency is also minimized. The notch shown in Figure 27 was sized to get the desired reduction in gain at the critical frequency.

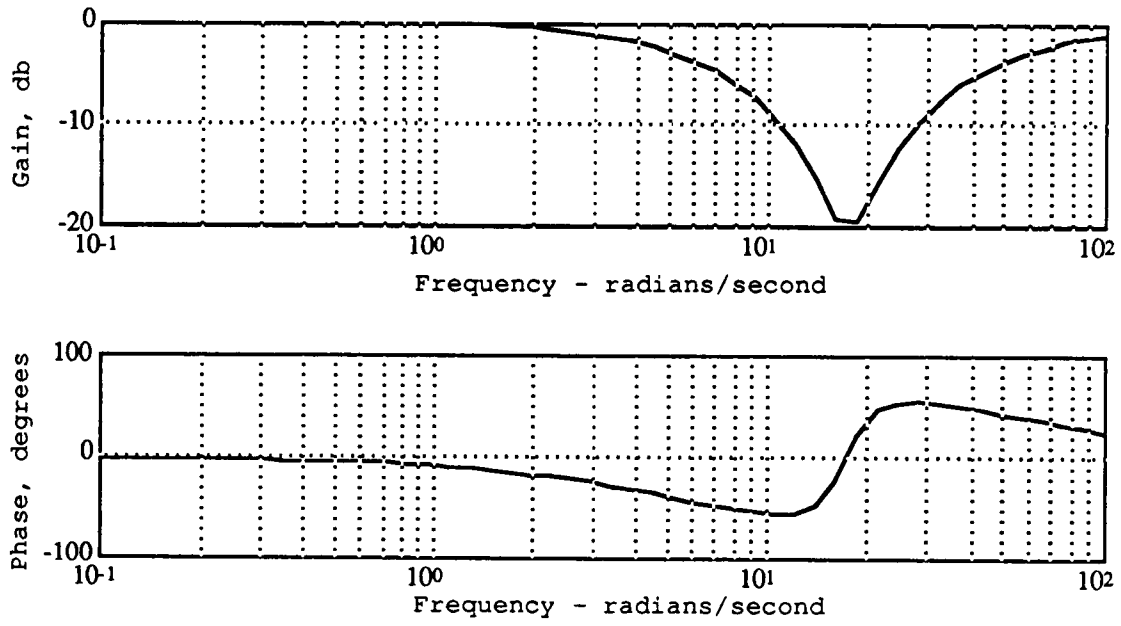

Figure 27. Frequency response of $\frac{s^2 + 2\zeta_{lag}\,\omega_n\,s + \omega_n^2}{s^2 + 2\zeta_{lead}\,\omega_n\,s + \omega_n^2}$ with ω_n=17.3, ζ_{lead}=1.5 and ζ_{lag}=0.15.

In Figure 26, the resonant peak at 17.3 rad/sec is about 14 dB. The notch filter was designed to attenuate the resonant peak by 20 dB gain at the resonant frequency. The resulting open-loop frequency response plot shown in Figure 28 exhibits a high gain margin and a gain of -5.5 dB at the resonant frequency.

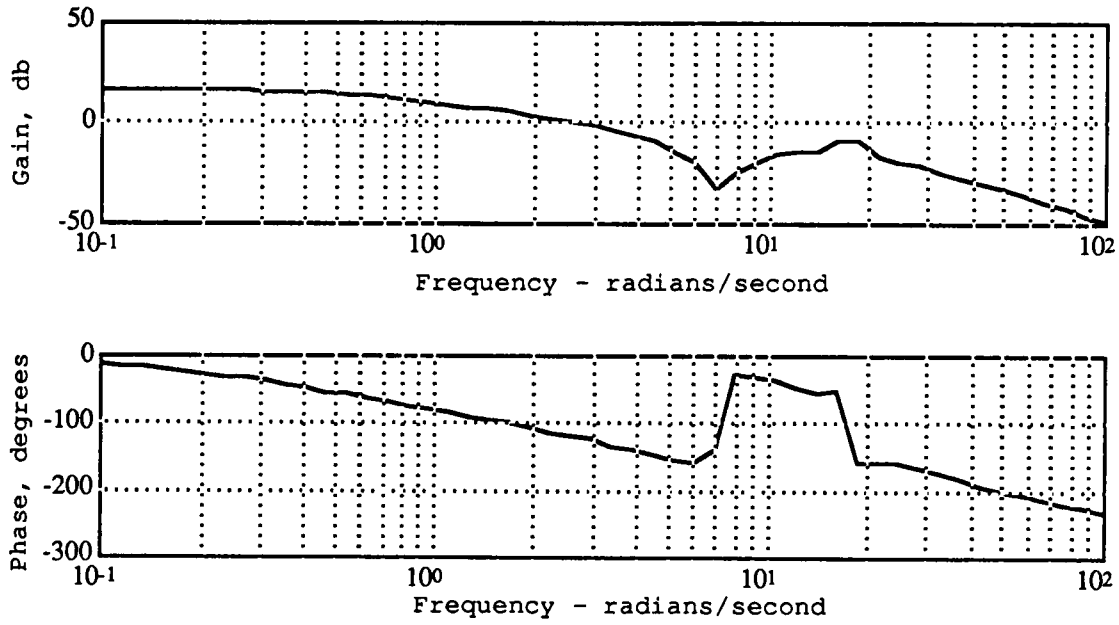

Figure 28. Open-loop frequency response of the system at 750 SHP with K_p=2.85, T_p=0.25, ω_n=17.3, ζ_{lead}=1.5 and ζ_{lag}=0.15.

Various values for the gains and time constants were tried on the plant at 750 SHP and are summarized in Table 6. To further attenuate the resonant peak, the compensator time constant (T_p) was increased to 0.4 sec. The resonant peak was

Table 6. Results of variation in compensator values for the plant at 750 SHP.

K_p	T_p	ω_n	ζ_{lead}	ζ_{lag}	GM	PM	BW	GR
2.85	0.25	17.3	1.5	0.15	23.03	63.16	2.79	-5.3
2.85	0.40	17.3	1.5	0.15	26.33	55.42	2.47	-9.4
2.85	0.25	17.3	0.4	0.04	9.85	77.82	3.0	-0.5
2.85	0.25	17.3	0.6	0.0	14.87	73.35	2.97	-5.0

attenuated to -9.4 dB. The additional phase lag still yields an acceptable phase margin, but the bandwidth has been reduced to about 2.5 rad/sec.

In addition to the notch shown in Figure 27, two other notches were evaluated. The notch with a lag of 0.04 and lead of 0.4 results in a system gain at the resonant peak of -0.5 dB which is not acceptable. Each set of compensator values shown in Table 6 produced acceptable results except in this case.

A notch in the form of

$$\frac{\frac{s^2}{\omega_n^2} + 1}{\frac{s^2}{\omega_n^2} + \frac{2\zeta_{lead}}{\omega_n} s + 1} = \frac{s^2 + \omega_n^2}{s^2 + 2\zeta_{lead}\,\omega_n\, s + \omega_n^2} \qquad (34)$$

was also tried. Since Equation 34 has infinite attenuation at ω_n, an actual implementation results in a small lag term in the numerator.

The compensator values shown in Table 7 provide stability without compromising system performance when applied to the system as shown in Figure 29.

TABLE 7. Gains and time constants selected for the coupled rotor system.

config	K_p	T_p	ω_n	ζ_{lead}	ζ_{lag}
CR	2.85	0.25	17.3	1.5	0.15

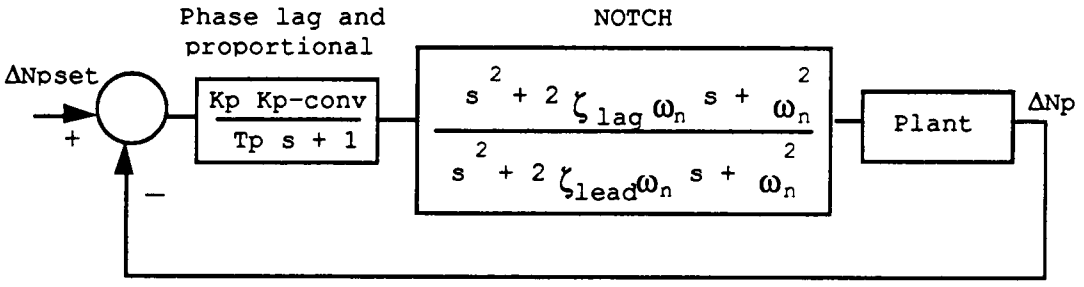

Figure 29. Block diagram showing compensator.

RESULTS AT EACH POWER LEVEL

Figure 30 shows the open loop frequency response, of the plant with the rotor coupled and the selected compensation from Table 7, at each of the power settings. All design goals were met, although the bandwidth was marginal. To attenuate the resonant peak to -6 dB limits the bandwidth to 3 rad/sec [13]. Therefore the bandwidth of 2.79, 2.41 and 2.11 rad/sec

for the 750, 500 and 250 SHP case, respectively is considered acceptable. Further improvement to the bandwidth will compromise the torsional stability.

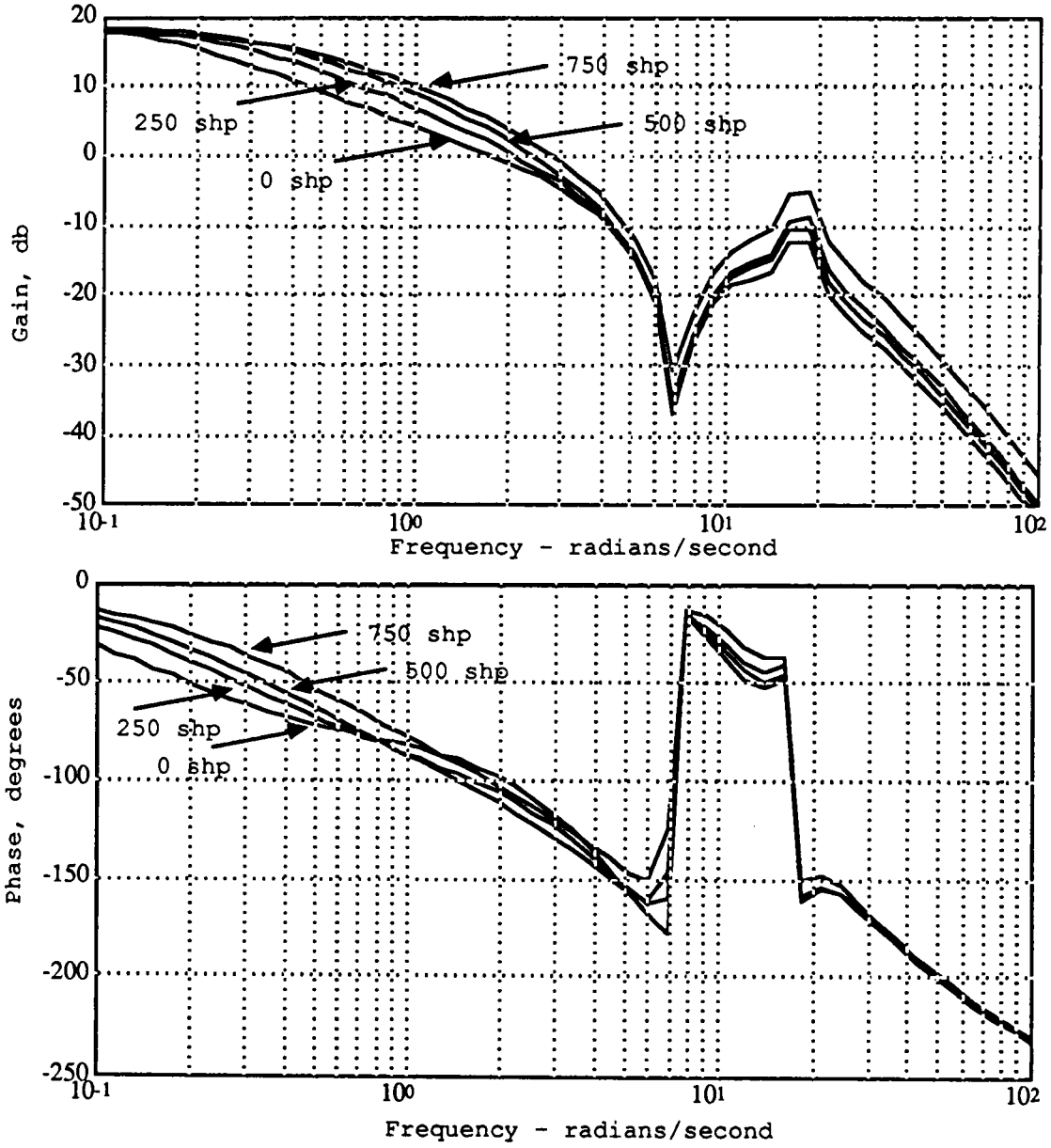

Figure 30. Open-loop frequency response of the system at each power level with selected compensation.

The closed loop step response shown in Figure 31 shows some ringing, which damps out. The steady-state error of 10% is considered acceptable. The results from adding the selected compensation to the plant at each power setting are summarized in Table 8.

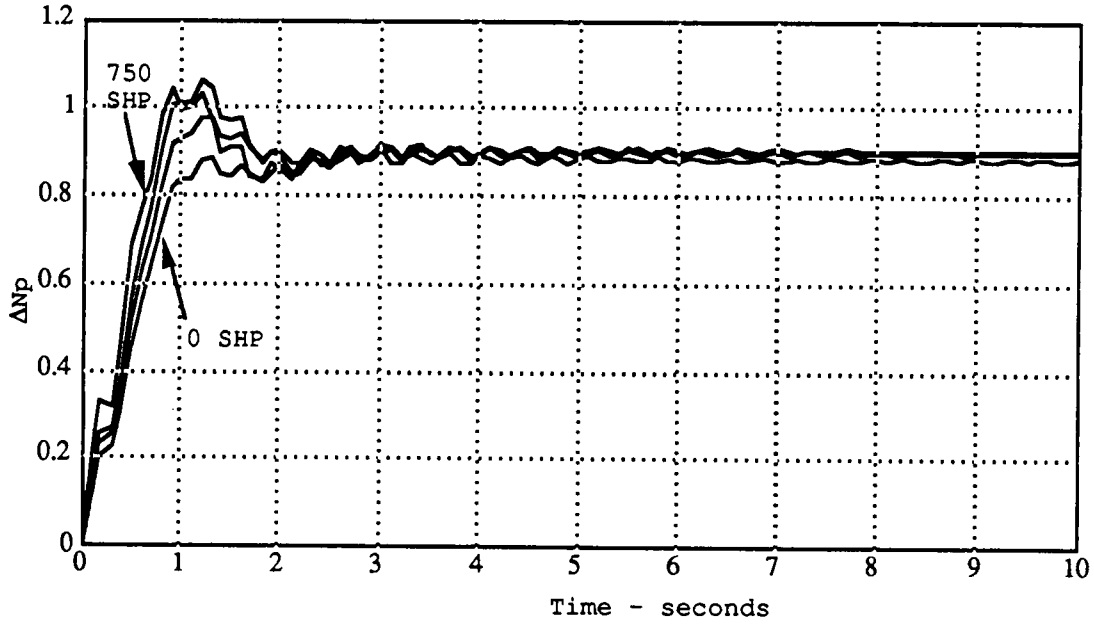

Figure 31. Closed-loop step response of the system at each power level with selected compensation.

TABLE 8. The final results for the coupled rotor system with selected compensator values.

config/SHP	GM dB	PM degrees	BW rad/sec	GR dB	ss-err %
CR/750	23.03	63.16	2.79	- 5.3	10
CR/500	29.39	61.02	2.41	- 9.2	10
CR/250	28.07	71.46	2.11	-10.5	10
CR/0	30.11	85.53	1.76	-12.4	12

RESULTS FOR THE DECOUPLED ROTOR

The compensator values chosen for the coupled rotor plant were also applied to the decoupled rotor case. The results were unacceptable as shown in Figure 32 because with the notch filter and the rotor decoupled, the stability margin is lost. The resulting gain margin is -0.54 dB and the phase margin is -2.52°. With the rotor decoupled and the engine in autorotation, the stability margin is lost. The torsional mode is not present and therefore the notch filter must be removed.

To determine the best stabilizing compensation for the decoupled rotor case, the response in Figure 19 was re-evaluated. The proportional and phase lag was changed and the notch filter removed. The proportional gain was reduced to 1.5 and a time constant of 0.2 sec chosen. Evaluation of the decoupled rotor without compensation had shown a high bandwidth and high phase margin but the gain margin was undefined. In Figure 33 enough phase was added to the system to get the phase to cross -180° and then enough gain was added to maintain the high bandwidth. The step response is shown in Figure 34. The results of applying compensation is summarized in Tables 9 and 10.

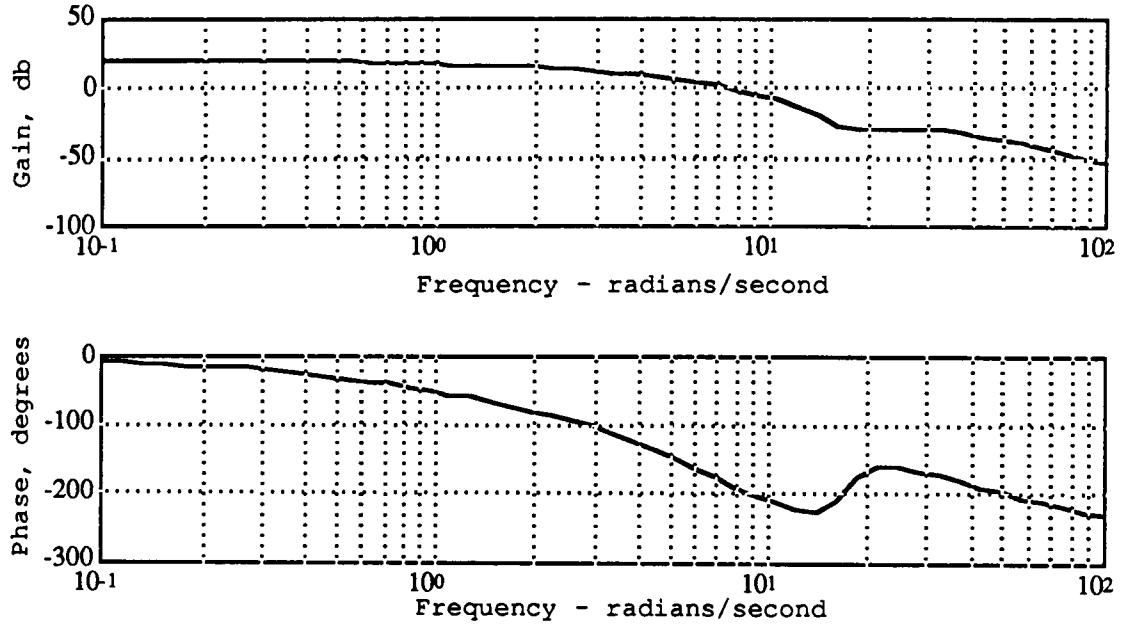

Figure 32. Open-loop frequency response of the decoupled rotor system with the compensation selected for the coupled rotor system.

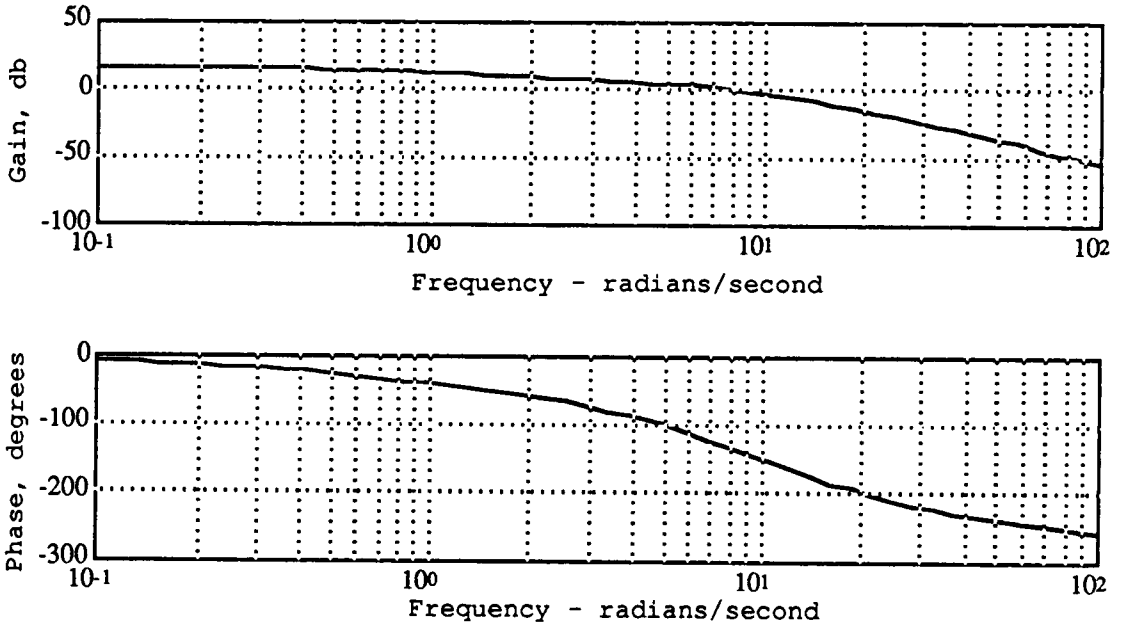

Figure 33. Open-loop frequency response of the decoupled rotor system with selected compensation.

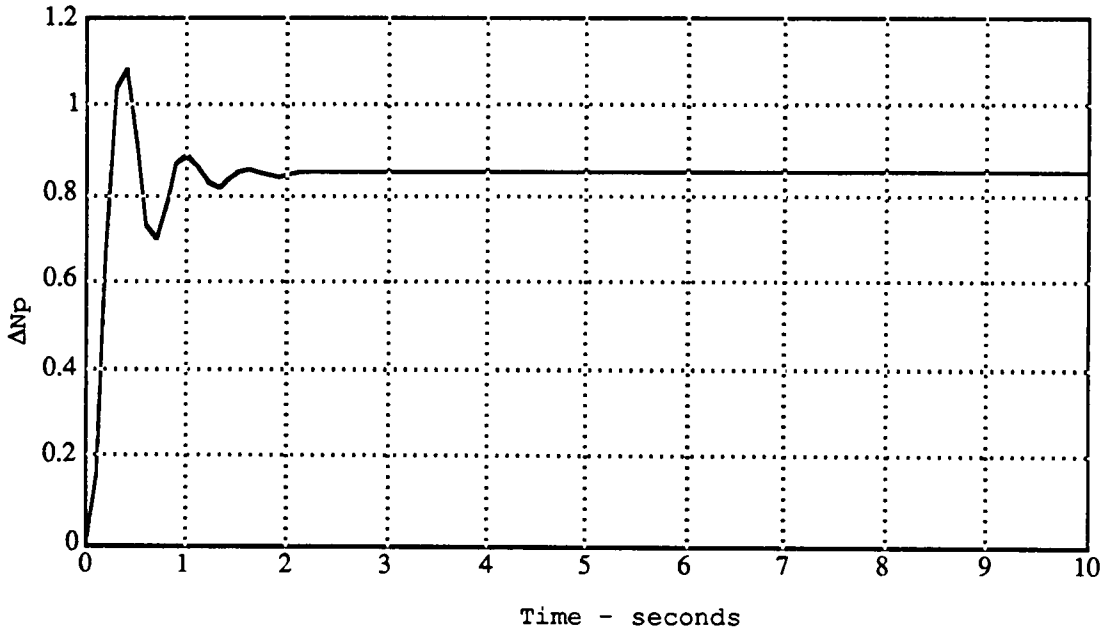

Figure 34. Closed-loop step response of the decoupled rotor system with selected compensation.

TABLE 9. Summary for the decoupled rotor system with the gains and time constants shown in Table 10.

config/SHP	GM dB	PM degrees	BW rad/sec	GR dB	ss-err %
DR/0	-0.54	-2.52	7.48	N/A	-
DR/0	9.39	44.58	8.25	N/A	14

TABLE 10. Gains and time constants for data in Table 9.

config	K_p	T_p	ω_n	ζ_{lead}	ζ_{lag}
DR	2.85	0.25	17.3	1.5	0.15
DR	1.5	0.2	N/A	N/A	N/A

FINAL RESULTS

The effect of adding compensation to the two configurations of the plant, CR and DR are summarized in Table 11, with corresponding gains and time constants shown in Table 12. Both provide satisfactory control for all power levels.

TABLE 11. The final results for the system with selected compensator values shown in Table 12.

config/SHP	GM dB	PM degrees	BW rad/sec	GR dB	ss-err %
CR/750	23.03	63.16	2.79	- 5.3	10
CR/500	29.39	61.02	2.41	- 9.2	10
CR/250	28.07	71.46	2.11	-10.5	10
CR/0	30.11	85.53	1.76	-12.4	12
DR/0	9.39	44.58	8.25	N/A	14

TABLE 12. Gains and time constants for data in Table 11.

config	K_p	T_p	ω_n	ζ_{lead}	ζ_{lag}
CR	2.85	0.25	17.3	1.5	0.15
DR	1.5	0.2	N/A	N/A	N/A

CHAPTER VI

DISCUSSION

The primary objective of this paper was to design a rotor speed governor for a prototype turboshaft engine to support a flight demonstration of the engine. Some of the major problems concerning engine and rotor system stability and performance were studied. To minimize development time and costs classical Bode and step response analysis were performed on a linearized model of the engine and rotor system to predict torsional stability and design stabilizing compensation. Resources describing helicopter control development are scarce; this thesis provides useful information for initial helicopter engine control development.

A controller was designed to:

1. provide accurate regulation of the rotor speed over the load ranges from zero to maximum shaft horsepower,

2. ensure stability with the high inertia rotor system coupled to the low inertia power turbine, and

3. ensure stability with the low inertia power turbine decoupled from the rotor system.

Design goals were selected and compensation determined which satisfied these requirements as follows:

1. Accurate control is provided with a bandwidth between 1.76 and 2.79 rad/sec and a steady state error between 10 and 12% for the coupled rotor and a bandwidth of 8.25 rad/sec and a steady state error of 14% for the decoupled rotor.

2. Stability for the coupled rotor case is provided by a torsional mode gain margin of between 23 and 30 dB and the low frequency phase margin between 61° and 85°. The low frequency 0 dB crossover point is high, indicating loop gain is high and the transient response has not been compromised to achieve stability.

3. Stability of the decoupled rotor case is provided with a low frequency gain and phase margin of 9.4 dB and 44.6°, respectively.

A practical design problem is to determine the effect on stability of variations in system parameters. Plots of the plant at each power setting show the coupled rotor system is fairly insensitive to parameter changes for the different levels of shaft horsepower. Therefore, the system was designed at the maximum shaft horsepower of 750 and then checked at 500, 250 and zero with good results.

To study the effects of rotor decoupling, the chosen compensation was applied to the decoupled rotor case. When the rotor is decoupled from the engine the notch filter is not required since the torsional mode oscillations are not present. In fact with the notch filter present the stability of the decoupled rotor is decreased. Therefore when "split-

needles" occurs the control must detect zero SHP and switch out the notch filter.

This paper discussed torsional stability of the coupled rotor to the engine, the effects of rotor decoupling, and the role the electronic control must play in stabilizing these effects. The chosen compensator design provides acceptable performance and stability for a development program and lays the ground work for further work. During the early concept testing of a demonstrator engine, a simple controller was needed to maintain fixed power turbine speed and ensure stability of the engine and rotor. For the production control additional factors will need to be investigated.

This paper concentrated only on the interaction between engine and rotor. Further control development must address other issues that effect the aircraft handling qualities. Future military helicopter engine controls require that the engine manufacturer consider the helicopters air combat agility and maneuverability. These considerations were not possible in an analog electronic control.

LIST OF REFERENCES

LIST OF REFERENCES

1. Coalson, M. S., "Status Report of the USAF's Engine Model Derivative Program", ASME, American Society of Mechanical Engineers Paper Number 82-GT-183, 1982. Page 2.

2. Needham, J. F., and Banerjee, D., Hughes Helicopters, "Engine/Airframe/Drive Train Dynamic Interface Documentation", USARTL-TR-78-12, May 1978. Pages 12-19.

3. Twomey, W. J., and Ham, E. H., Sikorsky Aircraft, "Review of Engine/Airframe/Drive Train Dynamic Interface Development Problems", USARTL-TR-78-13, June 1978. Page 112.

4. Richardson, D. A., and Alwang, J. R., Boeing Vertol Company, "Engine/Airframe/Drive Train Dynamic Interface Documentation", USARTL-TR-78-11, April 1978. Pages 100-115.

5. Sellers, J. F., and Baez, A. N., "Army/NASA Small Turboshaft Engine Digital Controls Research Program", American Helicopter Society Paper, Rotary Wing Propulsion System Specialist Meeting, November 1982. Pages 1-4.

6. Moler, C., Little, J., Bangert, S. and Cleiman, S., PC-MATLAB USER GUIDE, MathWorks, Inc., 1986.

7. Cohen, H., and Rogers, G. F. C., and Saravanamuttoo, H. I. H., Gas Turbine Theory, Longman Group Limited, 1972. Pages 2-6.

8. Harrison, H. L., and Bollinger, J. G., Introduction to Automatic Controls, International Textbook Co., 1969. Pages 329-330.

9. Doebelin, Ernest O., System Modeling and Response, John Wiley and Sons, 1980. Pages 565-570.

10. DiStefano, J. J., Stubberud, A. R., and Williams, I. J., Theory and Problems of Feedback and Control Systems, Schaum Publishing Co., 1967. (transformation #7) Page 115.

11. Reyes, G.De Los, and Gouchoe, D. R., "The Design of a Turboshaft Speed Governor Using Modern Control Techniques", NASA Report CR175046, February 1986. Pages 2-5.

12. Fredrickson, C., Rumford, K., and Stephenson, C., "Factors Affecting Fuel Control Stability of a Turbine Engine/Helicopter Rotor Drive System", American Helicopter Society Paper, 27th Annual National V/STOL Forum, May 1971. Page 2.

13. Howlett, J. J., Morrison, T., and Zagranski, R.D., "Adaptive Fuel Control for Helicopter Applications", American Helicopter Society Paper, Rotary Wing Propulsion System Specialist Meeting, November 1982. Page 5.

14. Society of Automotive Engineers Aerospace Recommended Practice A.R.P. 704, 1962.

15. Prouty, R. W., Practical Helicopter Aerodynamics, PJS Publications Inc., 1982. Pages 22-23.

16. Savant, C. J., Jr., Control System Design, McGraw-Hill Book, Inc., 1964. Pages 61-65.

17. Harrison, H. L., and Bollinger, J.G., Pages 15-16.

18. Warwick, T. W., "Helicopter Engine Dynamic Analysis", American Helicopter Society Paper, 25th Annual National Forum Proceedings, May 1969. Pages 2-3.

19. Gessow, A., and Myers, G. C., Jr., Aerodynamics of the Helicopter, N.Y.: Frederick Ungar, 1967. Page 276.

20. Kuczynski, W. A., Cooper, D. E., Twomey, W. J., and Howlett, J. J., "The Influence of Engine/Fuel Control Design on Helicopter Dynamics and Handling Qualities", American Helicopter Society Paper, 35th American Helicopter Association, May 1979. Page 2.

21. Harrison, H. L., and Bollinger, J. G., Page 218.

VITA

D. Leslie Burwell was born in Birmingham, Alabama on August 22, 1954. She graduated from Homewood High School in June 1973. In 1981, she graduated from the University of Alabama in Huntsville, with a Bachelor of Science in Engineering.

After graduating, she worked for CSC, Computer Sciences Corporation at Arnold Air Force Base in Tennessee. She entered graduate school on a part time basis and completed the requirements for a Master of Science degree with a major in Electrical Engineering in August 1990.

The author is currently working for Allied Signal Corporation, Garrett Engine Division in Phoenix, Arizona as a supervisor in the Turboprop Engine Controls group.